IOP Publishing Journal of Physics D: Applied Physics

J. Phys. D: Appl. Phys. **48** (2015) 494002 (18pp) doi:10.1088/0022-3727/48/49/494002

Long-term effects of multiply pulsed dielectric barrier discharges in air on thin water layers over tissue: stationary and random streamers

Wei Tian[1,3] **and Mark J Kushner**[2]

[1] University of Michigan, Department of Nuclear Engineering and Radiological Science, 2355 Bonisteel Boulevard, Ann Arbor, MI 48109-2104, USA
[2] University of Michigan, Department of Electrical Engineering and Computer Science, 1301 Beal Avenue, Ann Arbor, MI 48109-2122, USA

E-mail: bucktian@umich.edu and mjkush@umich.edu

Received 14 July 2015, revised 6 September 2015
Accepted for publication 24 September 2015
Published 16 November 2015

Abstract

Tissue covered by thin liquid layers treated by atmospheric pressure plasmas for biomedical applications ultimately requires a reproducible protocol for human healthcare. The desired outcomes of wet tissue treatment by dielectric barrier discharges (DBDs) depend on the plasma dose which determines the integral fluence of radicals, ions, electric fields and UV/VUV photons incident onto the tissue. These fluences are controlled by power, frequency and treatment time. To first order, these parameters determine the energy deposition (J cm^{-2}) onto the tissue. However, energy deposition may not be the only parameter that determines the fluences of reactants to the underlying tissue.
In this paper, we report on a computational investigation of multipulse DBDs interacting with wet tissue. The DBDs were simulated for 100 pulses at different repetition rates and liquid thicknesses followed by 10 s or more of afterglow. Two schemes were investigated—stationary and random. In the stationary scheme, the DBD plasma streamer continues to strike at the same location on the liquid layer, whereas in the random scheme the plasma streamer strikes at random locations on the liquid layer. These differences in streamer locations strongly affect the spatial distribution of solvated species such as OH_{aq} and H_2O_{2aq} ('$_{aq}$' represents an aqueous species), which have high rates of solvation. The spatial distribution of species such as NO_{aq}, which have low rates of solvation, are less affected by the location of the streamer due to the remediating effects of diffusion in the air. The end result is that fluences to the tissue are sensitive to the spatial location of the streamer due to the ensuing reactions in the liquid between species that have low and high rates of solvation. These reactions can be controlled not only through location of the streamer, but also by repetition rate and thickness of the liquid layer.

Keywords: dielectric barrier discharge, plasma on liquid, modeling, aqueous active species

(Some figures may appear in colour only in the online journal)

I. Introduction

Atmospheric pressure plasmas (APPs) are being investigated for healthcare-related applications including sterilization of medical equipment [1, 2], wound treatment [3, 4], cancer treatment [5, 6] and disinfection [7, 8]. The treatment of human tissue and wounds often occurs through an overlying liquid layer (the *wet wound*) through which plasma produced entities (radicals, ions, photons, electric fields) must penetrate before reaching the underlying tissue. Dielectric barrier discharges

[3] Present address: Applied Materials, 974 E. Arques Ave., Sunnyvale CA 94085, USA

(DBDs) represent one class of atmospheric pressure plasma widely used in clinical treatment due to their ability to treat large areas [9, 10]. Treatment of tissue using DBDs is often performed in a floating electrode mode where the tissue acts as one of the electrodes in the circuit. Hence, the characteristics of the tissue such as dielectric constant and conductivity can affect the discharge.

In treatment of wet tissue, the overlying liquid layer may be only hundreds of microns thick. However, even this thin layer is able to absorb the energetic electrons, ions and photons produced by DBDs, converting that activation energy into chemical reactivity which then transports to the underlying tissue. The majority of neutral species solvated into the liquid undergo reactions, such as conversion of hydroxyl radicals to hydrogen peroxide, prior to their reaching the tissue. The characteristics of the liquid layer, such as electrical conductivity and pH value are altered by long-term treatment by DBDs. For example, the conductivity of distilled water was increased by 100 μS cm^{-1} after 60 min of discharge treatment and the discharge characteristics were found to be sensitive to changes in the conductivity of the solution [11]. Double layers can occur at the surface of conductive liquids. This affects the electric field at the surface and influences the transport of charged species into the liquid. DBD treatment usually results in a reduction of pH value in the liquid layer [12, 13], although some studies [14] have reported an increase in pH value. The chemical reactivity of radicals in liquids is sensitive to these changes in pH.

There are many scenarios for applications of plasmas in contact with liquid. One of them is plasma-activated water (PAW) [15]. Water, after long-term contact with APPs, becomes an acidified and radical containing solution known as PAW. The water (or culture medium) is first activated by plasma treatment and the PAW is subsequently transferred to its intended use. This method has the advantage of not directly exposing the tissue, cells or medical equipment to the discharge and its associated high voltage. Graves and co-workers [15] reported on an indirect air DBD, the surface micro-discharge (SMD), in close proximity to water to produce PAW. The resulting PAW showed strong antibacterial activity for *Escherichia coli* one week after generation. The active species in PAW are presumably well mixed at the time of treatment and so the tissue being treated receives largely the same dose.

A second scenario is *in situ* tissue treatment as in the direct plasma treatment of wet tissue. The overlying liquid is typically water containing dissolved gases, salts and organic substances. This liquid layer processes plasma produced species and transfers them and their activation energy to the underlying tissue. Different from PAW, the liquid is typically thin and in direct contact with the tissue. This results in a rapid interaction of the plasma treated liquid with the tissue. By rapid we mean less than a second to a few seconds, compared to minutes to days in the case of PAW. In these cases of wet tissue with thin liquid layers, short-lived radicals can reach the tissue before they are fully processed by liquid layer whereas in PAW short-lived species will likely have already reacted prior to the final application. On the other hand, there are potentially active species that take minutes, and in some cases hours, to be generated. For example, after plasma treatment, the concentration of nitrate ions in PAW increased quickly from 1.2 mM to 3.0 mM within hours and then slowly to 5.0 mM in 7 d, while the concentration of nitrite ions in PAW diminished from 1.2 mM in 2 d [15]. Direct treatment of wet tissue would not necessarily produce these species in significant numbers. Having said that, prior studies have shown that even for water layers of a few hundred microns thickness, factors of two in layer depth, thinner or thicker, can produce significant differences in the fluences to underlying tissue [16].

In the context of plasma treatment of tissue covered by liquid, it is the reactive fluences (time integrated fluxes) reaching the tissue that ultimately determine the biomedical effects. The overlying liquid transforms the plasma produced reactive species before reaching the tissue. The details of this reactivity with tissue are the focus of current research [17–20]. Aqueous oxidants, such as O_{3aq}, OH_{aq} and H_2O_{2aq}, can chemically interact with cell components such as DNA, protein or lipid, leading to cell damage [21, 22]. (The subscript '$_{aq}$' denotes an aqueous species.) Cells contain small concentrations of antioxidants whose purpose is to prevent oxidants from reacting with, for example, DNA by donating electrons to the oxidants without becoming destabilized themselves. Oxidative stress is caused when oxidants and antioxidants are not in balance [23, 24]. When in contact with human cells, APPs usually produce oxidative stress by producing an overabundance of oxidizing species which transport into the cell. It is likely that a similar process occurs in the aqueous phase. Low-level oxidative stress can disrupt the normal mechanism of cellular signaling. More severe oxidative stress can cause cell death. Moderate oxidative stress can trigger apoptosis, while more oxidative stress may induce necrosis [25–27].

Nitrogen oxides also play an important role in biological systems [28–33]. NO_{aq} can induce oxidative stress when superoxide anions (O^-_{2aq}) are present in cells or in the medium surrounding cells [28, 29]. Reactions between NO_{aq} and O^-_{2aq} produce peroxynitrites, $ONOO^-_{aq}$, which are highly oxidative. NO_{aq} will eventually hydrolyze in water and become nitrous or nitric acids, which acidify the liquid layers in contact with cells, reducing the pH value, which in turn affects biological functions. The reactivity of peroxynitrites strongly depends on the pH value, becoming more reactive under acidic conditions [30]. The efficiency of deactivation of bacteria under acidic conditions could therefore be increased compared to less acidic conditions. NO_{aq} itself is also a major signaling agent for neurons and in immune systems [31]. At low concentrations, NO_{aq} acts as an anti-inflammatory agent preventing lipid peroxidation, reducing membrane permeability, and limiting cell apoptosis [32]. When produced in large excess, NO_{aq} can be neurotoxic. Experiments show that NO_{aq} can induce apoptosis of neuronal cells [33]. Other nitrogen oxides species, such a NO_{2aq}, NO_{3aq} and N_2O_{3aq}, are similar in function to NO_{aq} [34, 35].

Given the different potential outcomes on cells resulting from fluxes of different reactive oxygen and nitrogen species (RONS), there is a need to control the uniformity and

reproducibility of the reactive fluxes to ensure consistent treatment. A measure of reproducibility is the dose of plasma treatment, which typically refers to the time integrated fluxes of radicals, ions, photons and electric fields that are incident onto the liquid or tissue surface [36]. To first order, the dose should scale with the total energy deposition, J cm^{-2}, delivered to the surface. That energy deposition is a function of the power deposition (W cm^{-2}), pulse power waveform (pulse length) and pulse repetition frequency (PRF). However, there are strong second order effects, such as thickness of the liquid layer and time between pulses that influence the identity of the RONS incident onto the tissue. This implies that half the energy per pulse at twice the PRF does not necessarily deliver the same fluence (time integrated fluxes) of RONS as double the energy at half the PRF. In any event, dose increases with treatment time and it is typical that a few seconds to a few minutes are necessary to achieve significant bacterial sterilization [37, 38]. Bruggeman and co-workers [39] measured deactivation of *Pseudomonas aeruginosa* in 100 μl of saline solution as a function of treatment time. Deactivation was not observed until after 20 s of treatment, with longer treatment producing a rapid increase in the rate of deactivation. Although there is selectivity between normal cells and cancer cells or bacteria in their response to RONS, exposure to a high dose of plasma can also cause normal cell death [40].

In addition to treatment time, the dose can also spatially vary in DBDs. The plasmas in DBDs are often filamentary, which in turn produce spatially non-uniform reactive species. Typical DBDs have filaments that are hundreds of microns in diameter, although DBDs excited by short voltage pulses may appear to be uniform [41–43]. The typical DBDs used in plasma treatment, using microsecond pulses or AC sine-wave voltage, are filamentary [44–46]. In conventional DBDs, self-organization of filaments can produce nearly stationary patterns of plasma filaments with lateral spacing larger than the gap size [47, 48]. The spacing can be much larger than the diameter of an individual streamer. This self-organization can result in the same plasma filament striking the same location on the surface for an extended period of time. In other cases, the filaments may strike randomly, or slow movement of the applicator averages self-organized patterns over the surface. When treating liquid covered tissues, particularly when the thickness of the liquid is small, the spatial distribution of the filaments onto the surface may have a significant effect on the spatial distribution of reactive fluences onto the underlying tissue.

In this paper, we report on the results from a 2D computational investigation of multiply pulsed DBDs in contact with liquid covered tissue comprised of water with dissolved O_2. A 100-pulse, 100 Hz negative discharge in humid air, and its afterglow are investigated for the plasma produced reactivity in both the gas and liquid phase. The tissue underlying the liquid is modeled as a dielectric material with no conductivity. The liquid layer is computationally treated identically to gas as a partially ionized substance, but with a higher density and a specified permittivity. The same equations (e.g. continuity, energy, radiation transport, Poisson's equation) are solved in the gas phase and the liquid phase, albeit with different species and reaction mechanisms. To investigate the variability that may occur in DBD treatment of tissue, we modeled two extreme schemes—filaments that are stationary for 100 pulses and filaments that strike random locations on the liquid surface on each pulse.

We found that different solvation rates of gas phase species result in different spatial distributions of species entering the liquid. Gas phase species formed during the discharge pulse having large Henry's law constants for solvation enter the liquid near where the filament strikes. Gas phase species requiring many reactions and having a small Henry's law constant enter the liquid in a more spatially averaged manner. The spatial overlap between these two classes of species entering the liquid then differs between fixed and random streamers. For example, NO_{aq} is produced by solvation of NO from the gas phase. NO is formed by multiple reactions and has a low Henry's law constant, and so NO_{aq} is produced fairly uniformly over the surface of the liquid. OH in the gas phase is formed by a single reaction and has a large Henry's law constant. OH_{aq} is therefore produced in close vicinity of the streamer. When both NO_{aq} and OH_{aq} enter the liquid in the same location, NO_{aq} is rapidly depleted by reactions with OH_{aq}. With randomly striking streamers, little NO_{aq} survives to reach the tissue. For stationary streamers, NO_{aq} can reach the tissue a few streamers diameters away from where the streamer strikes.

We will briefly discuss the modeling platform used in this investigation in section II. In section III, we will discuss production of radicals and charged species in multiply pulsed DBDs, with a comparison of stationary and randomly striking streamers. Concluding remarks are presented in section IV.

II. Description of model

In this paper, we use the computer model, *nonPDPSIM* to investigate a DBD sustained in humid air interacting with a thin liquid layer covering an underlying tissue. The base case for the simulation addresses 100 pulses followed by 10 s of afterglow. Since the model is described in detail in [16, 49], it is only briefly discussed here. The simulation consists of a time integration of the continuity equations for gas phase and liquid phase species, while considering transport of these species between phases and radiation transport. For a given timestep, Poisson's equation and continuity equations are first simultaneously integrated for electric potential; and for densities of electrons and ions including surface charges. The densities of neutral species are then updated by solving neutral continuity equations. The electron temperature is obtained from integrating the electron energy conservation equation, where rate coefficients and transport coefficients for electrons in the gas phase are computed from local solutions of Boltzmann's equation for the electron energy distribution. In the liquid phase, the electron energy equation is not solved for and electron temperature is assumed to be the same as the liquid. This assumption will then preclude ionization and dissociation of liquid water that might occur by energetic electrons from the gas phase striking the surface of the water. Radiation transport of UV and VUV radiation into the water by relaxation of high-lying excited states of gas species is then

Table 1. Solubilities at 300 K and 1 atm [51, 52].

Species	Henry's law constant (mol L^{-1}-atm^{-1})
OH	25
H_2O_2	1.0×10^5
NO	1.9×10^{-3}
O_3	1.1×10^{-2}

addressed by using Green's function propagator. The differential equations were discretized using finite volume techniques with an unstructured mesh. Water vapor is allowed to evaporate from the liquid surface into the gas phase with its saturated vapor pressure, which is 27 Torr at 300 K [50].

From a neutral and charged particle transport perspective, the liquid phase is treated the same as the gas phase, albeit with a different reaction mechanism and different transport coefficients. For example, consider the numerical mesh point on the surface of the liquid. Fluxes moving into that mesh point from the gas phase use gas-phase transport coefficients. Fluxes moving from that mesh point into the liquid use liquid-phase transport coefficients. Since diffusivities and mobilities are approximately 1000 times smaller in the liquid phase, there can be an accumulation of species at the surface of the liquid. This is, in fact, the case with charged particles and electrons in particular. Electrons from the gas phase transport to the top of the liquid with gas phase rates and subsequently transport into the liquid with liquid phase rates. The accumulation at the surface produces what appears to be surface charging. In the absence of reactions which may deplete the surface resident charge, the surface charge is dissipated consistent with the dielectric relaxation time of the liquid.

Although our discharge pulse length and voltage rise time are short enough that the DBD may operate in a more uniform mode, our intent here is to investigate the filamentary mode of operation. The filamentary mode is produced by specifying as initial conditions a small spot of neutral plasma of magnitude 10^8 cm^{-3} at the surface of the top insulator.

Simulations were also performed while solving the electron energy equation in the water. For the conditions of interest, the E/N (electric field/neutral density) in the water is too small and the collision frequency too high for the electron temperature to significantly exceed that of the water. There was negligible dissociation and ionization produced by hot electrons in the water.

Henry's law constants for gas phase species and water for selected species are listed in table 1. Henry's law constant is a measure of the solubility of a gas phase species into a liquid. Henry's law only describes the dynamical equilibrium of solvation—the relative concentrations of the gas and liquid phase species at the interface. The actual rate of solvation is not necessarily known. In our model, the rate of solvation is given in analogy to the Noyes–Whitney formula [53],

$$\frac{dn_{aq}}{dt} = \frac{KD_g}{h}(hn_g - \min(n_{aq}, hn_g)) \qquad (1)$$

where n_{aq} is the density of the species at the surface of the water and n_g is the density of the species directly above the liquid in the gas phase. K is geometric factor which accounts for the spatial distribution of numerical mesh points, D_g is the diffusion coefficient in the gas phase, and h is the Henry's law constant. The implementation of equation (1) in the model is,

$$\frac{dn_{aqi}}{dt} = \sum_j \frac{D_{gij}A_{ij}}{d_{ij}V_i h}(hn_{gj} - \min(n_{aqi}, hn_{gj})), \qquad (2)$$

where n_{aqi} is the aqueous density at mesh point i and the sum is over adjacent mesh points j in the gas. n_{gj} is the gas phase density at mesh point j, A_{ij} is the area of the face of the numerical cell between points i and j, d_{ij} is the distance between points i and j, and V_i is the volume of the mesh cell surrounding i.

If the only source of the solvated species in the water is from the gas phase, then diffusion from the gas phase into the liquid stops when the equilibrium density of n_{aq} at the surface is reached. If the value of n_{aq} is reduced by either diffusion into the liquid or by reactions so that at the surface $n_{aq} < h \cdot n_g$, then solvation of gas phase species restarts. If diffusion of n_{aq} into the liquid from the surface is slow, solvation may slow to a negligible rate in spite of an abundance of gas phase species, since the density of n_{aq} at the surface is at equilibrium with the gas phase. This occurs even though n_{aq} may have a much smaller density deeper into the liquid and the average value of n_{aq} in the liquid layer is much smaller than the equilibrium value. All of the gas phase ions of interest have ionization potentials that are much larger than the surface energy or surface tension of the liquid. As a result, we assumed that ions are solvated without constraints.

In the absence of other data, Lennard-Jones parameters were used to compute diffusion coefficients in the liquid. This practice produces diffusion coefficients that are about 1000 times smaller in the liquid than in the gas phase. For example, the diffusion coefficient for NO in the gas phase is 0.22 cm^2 s^{-1} and in the liquid water is 1.75×10^{-4} cm^2 s^{-1}. The differences in diffusion coefficients for different species, such as OH and NO, vary by factors of 2–3, depending on their mass and Lennard-Jones parameters. However, the Henry's law constants for these species can vary by a factor of 10^4. The solvation rate of NO into the liquid is much slower than that of OH due to their relative Henry's law values and subsequent reactivity, and not because of large differences in their intrinsic rates of diffusion.

The Cartesian geometry used in this study is shown in figure 1, and represents a DBD sustained in humid air over liquid covered tissue. The computational domain is 6 mm × 4 mm. The powered electrode is at the top and covered by an insulator 0.12 mm thick with a dielectric constant of $\varepsilon/\varepsilon_0 = 3$. Under the insulator is a 1.5 mm gas gap filled with humid air ($N_2/O_2/H_2O = 79.0/20.9/0.1$) at 1 atmosphere pressure. The tissue beneath the gap is treated as a lossy dielectric with dielectric constant of $\varepsilon/\varepsilon_0 = 6$ and the bottom of the tissue is in contact with a grounded metal plate. A 200 μm thick liquid layer covers the tissue and is in contact with the gas. The layer consists of liquid water with a density of 3.32×10^{22} cm^{-3} and 8 ppm of pre-dissolved O_{2aq}, which is in equilibrium with the O_2 in the gas phase. The liquid is initially not conductive. However, its conductivity naturally

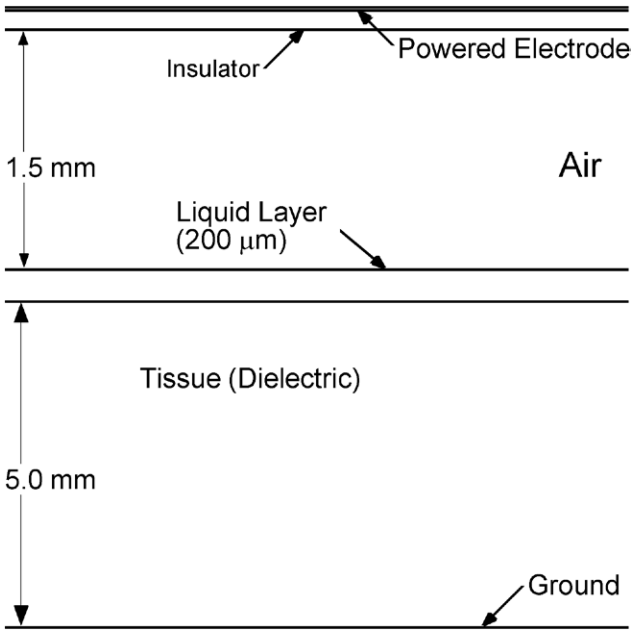

Figure 1. Schematic of the geometry where the plasma interacts with the liquid layer covering tissue. The total computational domain is 6 mm × 4 mm.

increases during treatment as the discharges produce ions in the liquid. Reactive species reaching the underlying tissue through the liquid are uniformly consumed. An unstructured mesh is used with refinement regions along the insulator and in the liquid layer. The mesh size varies from 20 μm along the insulator and liquid surface to 50 μm in the remote gas gap. The spacing of the mesh in the liquid layer is not able to resolve double layer structures.

Computing the electric discharge properties while solving Poisson's equation and charged particle dynamics is computationally intensive. A direct computation of Poisson's equation and charged particle dynamics for hundreds of pulses would be computationally prohibitive. In our model, the first discharge pulse is fully computationally resolved by solving Poisson's equation, all charged and neutral particle dynamics, and the electron energy equation for a duration of 10 ns. At the end of the first pulse, the source terms, such as the production terms for species and radiation transport, are recorded. During the interpulse period, Poisson's equation is not solved and we assume quasi-neutral conditions. The reaction mechanism during the interpulse period is identical to that during the discharge pulse—that is, we continue to include all reactions for charged particles and neutral both in the gas phase and in the liquid. Since the thermalization time for the electron temperature at atmospheric pressure is at most a few ns, the electron temperature during the afterglow is set equal to the ambient gas temperature. During the afterglow, the electrons solvate in the liquid within ns and attach in the gas phase in tens of ns, leaving a negative ion–positive ion plasma. Other than the small ambipolar electric field required to maintain charge neutrality, the electric field is otherwise set to zero during the afterglow.

At the end of the 10 ms interpulse period the electron density has decayed to negligible values as its 3-body attachment to O_2 occurs in less than 100 ns. The plasma that remains at the beginning of the next pulse is essentially an ion–ion plasma having a density of 10^8–10^9 cm^{-3}. For discharge pulses after the first, Poisson's equation is not solved. Instead the recorded electron impact source terms produced during the first pulse are introduced into the gas gap and liquid to represent the production of species by the next discharge pulse. Since the interpulse period is 10 ms (or longer) and the discharge pulse is 10 ns, these electron impact sources appear to be instantaneous on the time scale of the interpulse period even during the first fully resolved discharge pulse. Therefore, the level of approximation by having source terms appear instantaneously in pulses after the first pulse is not severe. This method enables a large increase in timestep during the afterglow. The integration timestep is dynamically chosen at all times in the simulation based on factors such as the Courant limit and the dielectric relaxation time. During the discharge pulse, the integration timestep is as small as 1 ps. During the afterglow, the timestep is as large as 10 μs.

Since the same source terms are used to represent successive pulses, from a plasma dynamics perspective, the 100 discharge pulses are identical and do not reflect changes in the composition of the gas. With successive pulses, long-lived species such as O_3 and NO accumulate in the gas gap, mixing with the air. In the liquid layer, ions such as $H_3O^+_{aq}$ and NO^-_{3aq} accumulate and the liquid becomes conductive. These long-term effects could influence later discharge pulses. However, the described level of approximation is required in order to simulate the hundreds of pulses needed to achieve quasi-steady state values of species in the liquid.

III. Multipulse DBD treatment of wet tissue

The complete liquid reaction mechanism is discussed in [16]. A subset of the reactions is shown in table 2 and is discussed here. The majority of O_{3aq} results from solvation of O_3 from the gas phase. In the liquid phase, O_{3aq} can be produced through O_{aq} reacting with dissolved O_{2aq}. However, since the flux of O atoms entering the liquid is small, little O_{aq} is produced through this channel. O_{3aq}, with an oxidation potential of 2.07 eV, eventually dominates the ROS in the liquid layer after many pulses. In the gas phase, •OH is dominantly produced by electron impact dissociation of H_2O. The •OH then either solvates in the water or forms H_2O_2 through mutual reactions. In the liquid phase, $\bullet OH_{aq}$ is also produced in significant amounts through photolysis of H_2O_{aq}. As in the gas phase, H_2O_{2aq} is created through mutual reactions of $\bullet OH_{aq}$ and is relatively stable compared to $\bullet OH_{aq}$ in the absence of organics. H_2O_{2aq} with an oxidation potential of 1.77 eV, compared to 2.85 eV for $\bullet OH_{aq}$, is able to survive long enough to transport through the liquid. NO is the initiating species for the formation of nitrogen oxides, N_xO_y (NO, NO_2, N_2O_3, N_2O_4 and N_2O_5), and acids, HNO_x (HNO_2 and HNO_3). Since many gas phase reactions are required to form the higher N_xO_y and HNO_x, these species solvate into the liquid during the afterglow after discharge pulses. Once in the liquid, N_xO_{yaq} either quickly reacts with OH_{aq} to form HNO_{xaq}

Table 2. Selected aqueous reactions.

Reaction[a]	Rate coefficient[a]	Reference
$O\bullet_{aq} + O_{2aq} \rightarrow O_{3aq}$	3×10^9	[54][b]
$\bullet OH_{aq} + \bullet OH_{aq} \rightarrow H_2O_{2aq}$	5.5×10^9	[54]
$NO_{aq} + NO_{aq} + O_{2aq} \rightarrow NO_{2aq} + NO_{2aq}$	2.3×10^6 M^{-2} s^{-1}	[55]
$NO_{aq} + NO_{2aq} + H_2O_{aq} \rightarrow HNO_{2aq} + HNO_{2aq}$	2×10^8 M^{-2} s^{-1}	[55]
$NO_{aq} + \bullet OH_{aq} \rightarrow HNO_{2aq}$	2×10^{10}	[55]
$NO_{aq} + HO^{\bullet}_{2aq} \rightarrow HNO_{3aq}$	8×10^9	[55]
$NO_{2aq} + \bullet OH_{aq} \rightarrow HNO_{3aq}$	3×10^{10}	[55]
$NO_{aq} + HO^{\bullet}_{2aq} \rightarrow HOONO_{aq}$	3.2×10^9	[55]
$NO_{2aq} + \bullet OH_{aq} \rightarrow HOONO_{aq}$	1.2×10^{10}	[55]
$NO^-_{2aq} + O_{3aq} \rightarrow NO^-_{3aq} + O_{2aq}$	5.0×10^5	[55]
$HNO_{2aq} + H_2O_{aq} \rightarrow H_3O^+_{aq} + NO^-_{2aq}$	1.8×10^1	[56][c]
$H_3O^+_{aq} + NO^-_{2aq} \rightarrow HNO_{2aq} + H_2O_{aq}$	1.8	[56][c]
$HNO_{3aq} + H_2O_{aq} \rightarrow H_3O^+_{aq} + NO^-_{3aq}$	2×10^3	[56][c]
$H_3O^+_{aq} + NO^-_{3aq} \rightarrow HNO_{3aq} + H_2O_{aq}$	2×10^2	[56][c]
$N_2O_{3aq} + H_2O_{aq} \rightarrow HNO_{2aq} + HNO_{2aq}$	1.1×10^4	[55]
$N_2O_{4aq} + H_2O_{aq} \rightarrow HNO_{2aq} + HNO_{3aq}$	8×10^2	[55]
$N_2O_{5aq} + H_2O_{aq} \rightarrow HNO_{3aq} + HNO_{3aq}$	1.2	[55]
$NO_{2aq} + NO_{2aq} + H_2O_{aq} \rightarrow HNO_{2aq} + H_3O^+_{aq} + NO^-_{3aq}$	1.5×10^8 M^{-2} s^{-1}	[56]
$NO_{2aq} + NO_{2aq} + H_2O_{aq} \rightarrow H_3O^+_{aq} + NO^-_{2aq} + H_3O^+_{aq} + NO^-_{3aq}$	5×10^7 M^{-2} s^{-1}	[56]
Photon reactions		
$h\nu + H_2O_{aq} \rightarrow H^{\bullet}_{aq} + \bullet OH_{aq}$	1×10^{-20} cm^2	[57][b]

[a] Aqueous species have an 'aq' subscript. Rate coefficients have units of M^{-1} s^{-1} (l•mole^{-1} s^{-1}) unless noted otherwise. '•' represents a free radical.
[b] Approximated by analogy.
[c] The rate coefficient is estimated according to thermodynamic hydrolysis in liquid water.

or slowly reacts with H_2O_{aq} to form HNO_{xaq}. Nitrogen acids, HNO_{2aq} and HNO_{3aq}, will hydrolyze in the liquid and produce hydronium, $H_3O^+_{aq}$, and their conjugate ions, NO^-_{2aq} and NO^-_{3aq}. Nitrous acid, HNO_{2aq}, is a weak acid and only a few percent hydrolyzes, while HNO_{3aq} is a strong acid and nearly completely hydrolyzes. With O_{3aq} in the liquid, NO^-_{2aq} is slowly oxidized to NO^-_{3aq} by reactions with O_{3aq} which assists the hydrolysis of nitrous acid.

The evolution of a DBD discharge during the first pulse is shown in figure 2, where the electron density, n_e, and electron impact ionization source, S_e, are shown. A −18 kV pulse with rise time of 0.1 ns and duration of 10 ns was applied to the powered electrode at the top of the domain. A neutral plasma (electrons and N^+_2) with a density of 10^8 cm^{-3} and diameter of 100 μm was placed adjacent to the middle of the insulator to initiate the plasma, after which the plasma self-sustains by gas phase and secondary processes on the surface. The magnitude of the seed electrons does not affect the properties of the plasma streamer with a factor of 10 larger or smaller density. After applying the pulse, the negative avalanche begins from the seed electron cloud and propagates downward. At 2.5 ns, the plasma streamer with an electron density of 2×10^{13} cm^{-3} strikes the liquid layer and a restrike avalanche proceeds backwards to the upper insulator. S_e reaches 9×10^{22} cm^{-3} s^{-1} at the head of the backward streamer. After 5 ns, the top insulator is nearly full charged and a conductive channel forms across the gap. Plasma then begins to spread over the surface of the insulator. The electron density is maximum at 2×10^{14} cm^{-3} and S_e is 2×10^{23} cm^{-3} s^{-1} adjacent to the insulator. The electron density at the surface of the liquid reaches 10^{14} cm^{-3}. These electrons quickly solvate into the liquid.

In pulses following the first, the source terms obtained from the fully resolved first discharge pulse are placed in the gap. As mentioned above, two extremes are discussed in this work, illustrated in figure 3, which shows the electron density in a subset of the computational domain. In the stationary scheme, the plasma streamer strikes at the same location on the surface of the liquid for all pulses. In the second scheme, the streamer randomly strikes the liquid on a pulse-to-pulse basis. The 1st, 54th and 88th pulses shown in figure 3(b) are intended to show that the locations at which the streamers randomly strike can be separated by many streamer diameters.

The resulting spatial distributions in the gas phase of quickly formed and solvating species (e.g. OH and H_2O_2), and slowly formed and solvating species (e.g. N_xO_y) significantly differ. For example, the sum of the densities of OH and H_2O_2, N_xO_y and O_3 are shown in figure 4 after the 1st, 54th and 88th pulses for stationary and random streamers. The OH is formed by direct electron impact dissociation of H_2O vapor and H_2O_2 is formed with one reaction between OH radicals. Their densities are maximum, $\approx 10^{13}$ cm^{-3}, adjacent to the water where the saturated water vapor has its highest densities. Both of these species quickly solvate into the liquid. OH, in particular, is also reactive with gas phase species (such as NO_2 in the formation of HNO_3) with nearly gas kinetic rate coefficients. As a result, OH and H_2O_2 do not significantly accumulate in

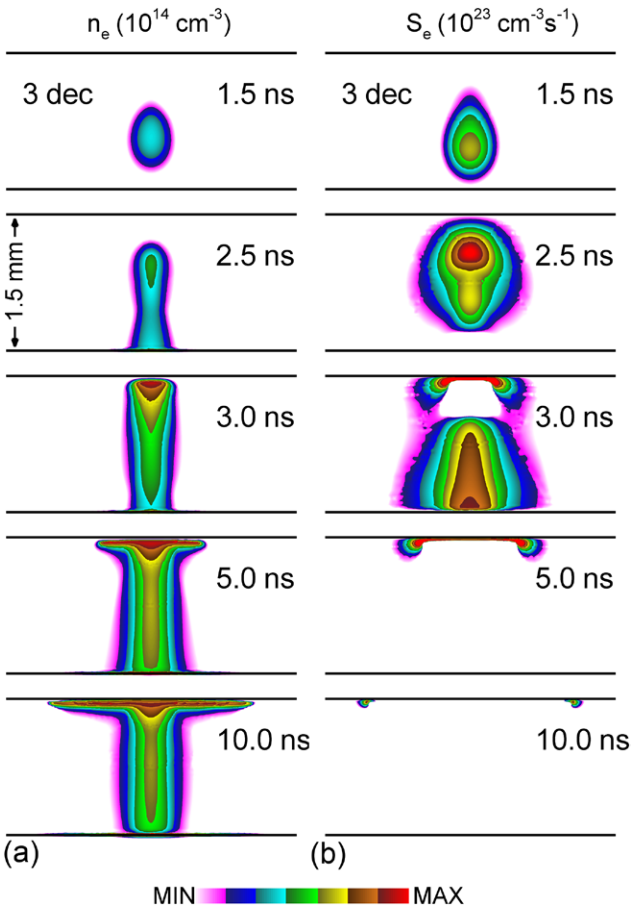

Figure 2. Time evolution of (a) electron density, n_e, and (b) electron impaction ionization source, S_e, for a negative discharge operated at −18 kV for 10 ns over a 200 μm water layer. Only the gas gap is shown. The initial gas is 1 atm, $N_2/O_2/H_2O$ = 79.9/20/0.1, and water evaporates from the surface. The contours for n_e and S_e are plotted on a log scale over three decades with maximum values shown at the top.

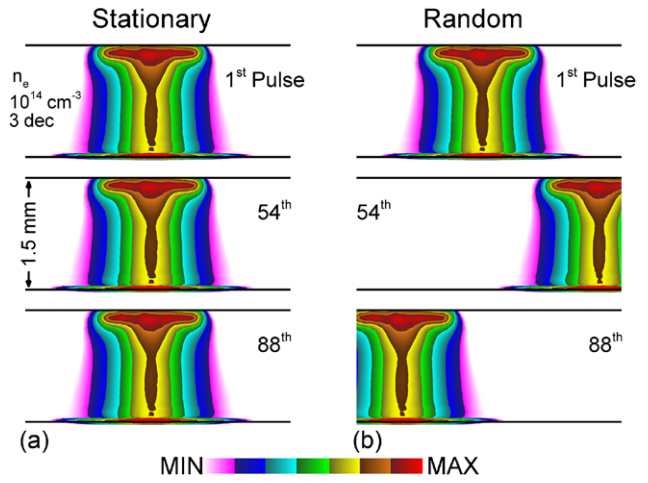

Figure 3. Stationary and randomly striking streamers represented by electron density in the gas gap. (a) Stationary scheme in which the plasma streamer continues to strike at the same location of the liquid layer on a pulse-to-pulse basis. (b) Random scheme where the plasma streamer strikes at a different location on the liquid layer on a pulse-to-pulse basis. The contours are plotted on a three-decade log-scale with the maximum values noted in each frame.

the gas phase. The solvation of these species into the liquid basically occurs at the location where the streamer strikes the surface.

The nitrogen oxides (N_xO_y) do not quickly solvate into the liquid due to their small Henry's law constants. Many reactions are required to form the higher N_xO_y in the gas phase, which requires additional residence time in the gas phase. The end result is that N_xO_y accumulates and diffuses in the gas phase, before solvating and retains little memory of where the plasma streamers hit. This accumulation is shown in figure 4, where the average gas phase density of N_xO_y after 100 pulses exceeds 10^{13} cm^{-3}. Even for the stationary streamer, there is a broad distribution of N_xO_y due to its diffusion during the interpulse periods. The composition of N_xO_y is about 90% NO.

The evolution over successive pulses of gaseous ozone (O_3) is shown in figure 4(c). Similar to the nitrogen oxides, O_3 accumulates in the gas phase. O_3 is primarily produced by O reacting with O_2. With a Henry's law constant of 0.011 mol L^{-1} atm^{-1}, O_3 solvates into the liquid faster than nitrogen oxides. However, its rate of solvation is still much lower than OH and H_2O_2. Therefore, the accumulation of O_3 is not severely affected by the locations where the plasma streamer strikes the liquid surface. The peak density of O_3 reaches as high as 10^{15} cm^{-3} and average density exceeds 10^{14} cm^{-3} after 100 pulses. In our mechanism about 10% of O_3 reacts with the upper dielectric and so the density of O_3 decreases near the wall. In the gas phase, there is no significant depletion of O_3 except for solvating into the liquid layer. As a result, virtually all O_3 will eventually be solvated into the liquid to form O_{3aq}.

The evolution of H_2O_{2aq} and NO_{aq} over 100 pulses (5th, 10th, 50th and 100th pulses) is shown in figure 5(a) for stationary streamers and in figure 5(b) for randomly striking streamers. OH_{aq} is largely formed where the streamer strikes the liquid through photolysis of water by UV/VUV photons or solvation of gaseous OH, both of which reflect the diameter of the streamer. The source of OH_{aq} being local to the streamer is exacerbated by charge exchange reactions of gas phase ions with H_2O_{aq}. The gas phase ions do not diffuse far from the streamer before entering the liquid. The charge exchange reactions with liquid H_2O_{aq} produce $H_2O^+_{aq}$, which then charge exchanges with H_2O_{aq} to form $H_3O^+_{aq}$ and OH_{aq}. Photoionization reactions which produce $H_2O^+_{aq}$ also occur only in the direct vicinity of the streamer. OH_{aq}, whose density at the surface of the liquid has a maximum of 9.5×10^{14} cm^{-3}, reacts with a sub-millisecond lifetime. In pure water, OH_{aq} is dominantly depleted by formation of H_2O_{2aq} through mutual reaction, and whose density accumulates to 10^{16} cm^{-3} at the surface of the liquid. OH_{aq} is depleted so rapidly that its density is not easily shown in figure 5. The trace of where OH_{aq} was formed is the resulting density of H_2O_{2aq}.

As NO_{aq} and N_xO_{yaq} are formed at the surface of the liquid, reactions with the surface resident OH_{aq} quickly occur. As N_xO_y only slowly solvates into the liquid, the initial distribution of N_xO_{yaq} is fairly uniform reaching densities of 5×10^{15} cm^{-3} at the surface. The reactivity of H_2O_{2aq} with N_xO_{yaq} is much

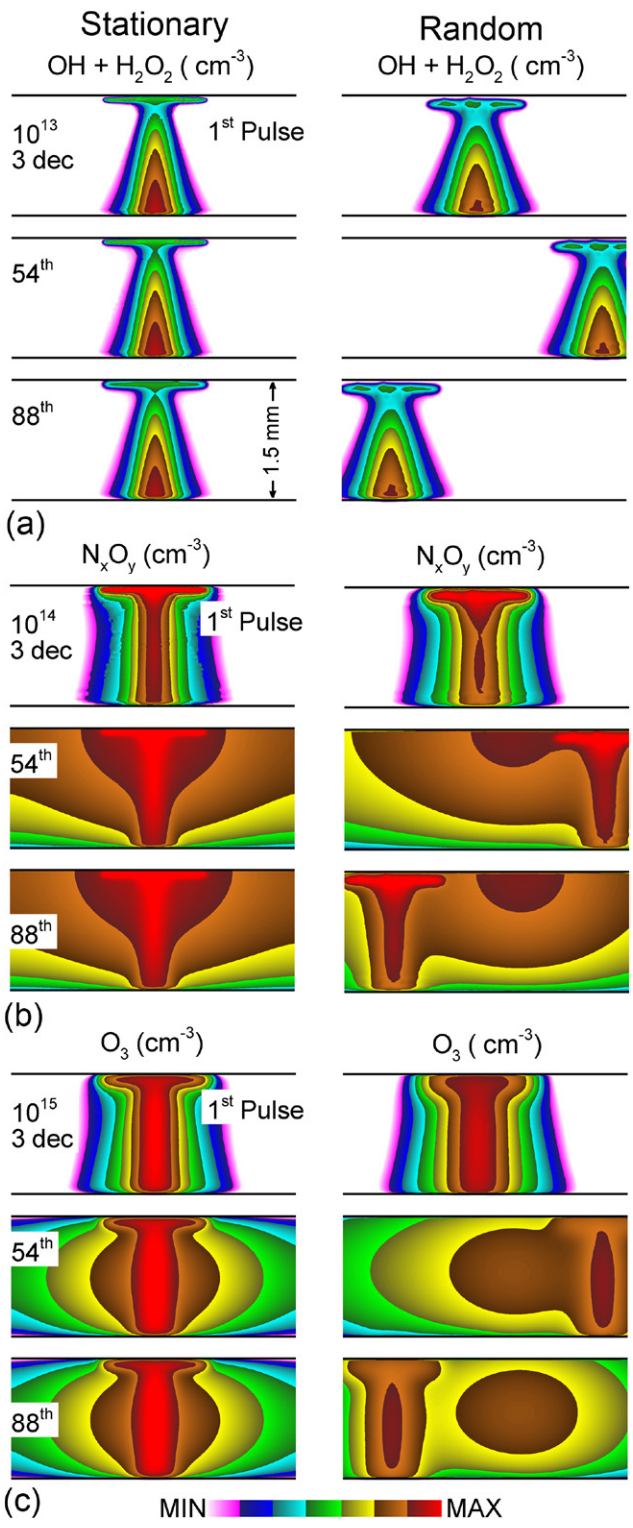

Figure 4. Densities of OH, H_2O_2, N_xO_y (sum of NO, NO_2, N_2O_3, N_2O_4 and N_2O_5) and O_3 in the gas gap at the beginning of the 1st, 54th and 88th pulse for the stationary and random schemes. The contours are plotted on a three-decade log-scale with the maximum values noted in each frame.

lower than for OH_{aq}, and so H_2O_{2aq} can accumulate and transport through the liquid to reach the underlying tissue. There is a wider distribution of H_2O_{2aq} (5th pulse) before a significant amount of NO_{aq} is solvated. After 10 pulses, when NO_{aq} begins to appear in the liquid, the distribution of H_2O_{2aq} is narrowed. This narrowing results from the consumption of OH_{aq} by reactions with N_xO_{yaq} and NO_{aq} in particular. Since H_2O_{2aq} only slowly reacts with NO_{aq}, H_2O_{2aq} begins to laterally expand by free diffusion after 80 pulses. For thin water layers, this lateral diffusion is not great, and so the flux of H_2O_{2aq} to the underlying tissue is localized under the streamer.

The rate of solvation of NO is much lower than for OH, and NO spreads in the gas gap prior to solvation. As a result NO_{aq} solvation occurs along the entire surface even for a stationary streamer. Since the source of NO_{aq} is only from NO solvation as it cannot be initially produced locally in the liquid, the initial distribution of NO_{aq} mirrors that of NO in the gas phase. However, directly under the streamer where OH_{aq} is produced, NO_{aq} is nearly completely consumed by its conversion to nitrous and nitric acids by reaction of OH_{aq}. At locations a few streamer radii distant from where the streamer strikes, the density of OH_{aq} is sufficiently small that NO_{aq} can diffuse away from the surface without reacting with OH_{aq}. This NO_{aq} eventually reaches the underlying tissue by the 50th pulse (0.5 s). This disparity in the disposition of NO_{aq} and H_2O_{2aq}, could for example, produce an overdose of H_2O_{2aq} and an underdose of NO_{aq} at the location where the streamer strikes. Elsewhere the situation would be reversed.

The evolution of H_2O_{2aq} and NO_{aq} over 100 pulses with randomly striking streamers is shown in figure 5(b). With randomly striking streamers, both OH_{aq} and NO_{aq} are initially formed across the entire surface of the liquid. The resulting density of H_2O_{2aq} at the surface,$\approx 10^{15}$ cm^{-3}, is about an order of magnitude smaller than under the stationary streamer as its formation is now averaged over the entire surface instead of being concentrated in a single location. The initially uniform distribution of NO_{aq} solvating into the liquid results from its low reactivity in the gas phase and low rates of solvation into the liquid. The initial distribution of OH_{aq} at the surface of the liquid is produced from an accumulated average of the randomly striking streamers which results in solvation of OH_{aq} or formation of OH_{aq} in the water under the streamer. These impulsive sources of OH_{aq} occur randomly, but discretely, across the surface of the liquid. It is for this reason that the distribution of H_2O_{2aq} is not perfectly smooth—it reflects the discrete injections of OH_{aq} with each randomly placed pulse. The now fairly uniform distribution of OH_{aq} consumes NO_{aq} in about 0.3 ms, before NO_{aq} can diffuse away from the surface. Since the OH_{aq} is now fairly uniformly formed at the surface and NO_{aq} uniformly enters the liquid, little NO_{aq} survives reactions with OH_{aq} to reach the tissue below. NO_{aq} can only be seen in significant amounts at the surface of the liquid with a density of 10^{14} cm^{-3}, a factor of nearly 50 times smaller than that in the case of the stationary streamer (see figure 5(b)). After 5 pulses, the density of H_2O_{2aq} is 10^{15} cm^{-3} and concentrated at the liquid surface before diffusion distributes the density. After 10 pulses, diffusion of H_2O_{2aq} begins to homogenize its density. After 100 pulses, there is little NO_{aq} in the bulk liquid whereas H_2O_{2aq} eventually reaches the tissue across the entire surface. NO solvation is slow but continues on a pulse-to-pulse basis and so NO_{aq} continues to be produced. This steady production of NO_{aq} consumes OH_{aq}, which

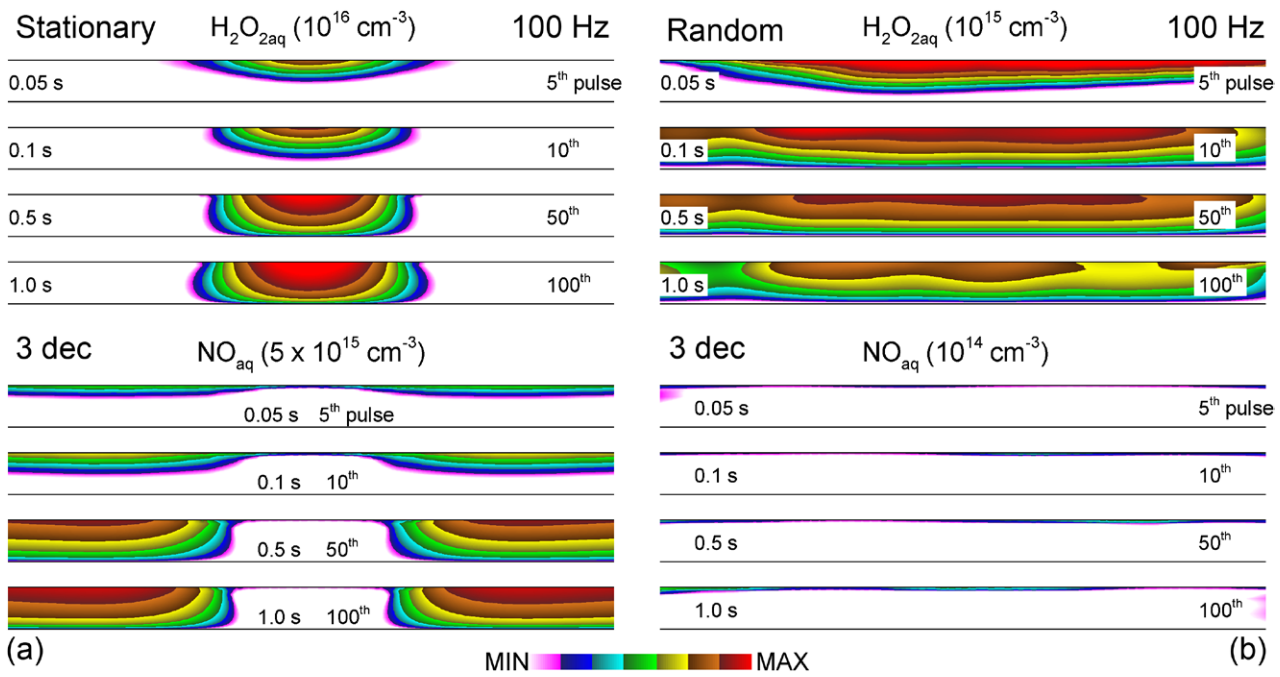

Figure 5. The time evolution of H_2O_{2aq} and NO_{aq} densities in the 200 μm water layer ('$_{aq}$' represents an aqueous species) at the end of the 5th, 10th, 50th and 100th pulse for (a) stationary streamers and (b) randomly striking streamers. The time and corresponding pulse number are shown in each frame. The contours are plotted on a three-decade log-scale with the maximum values at the top.

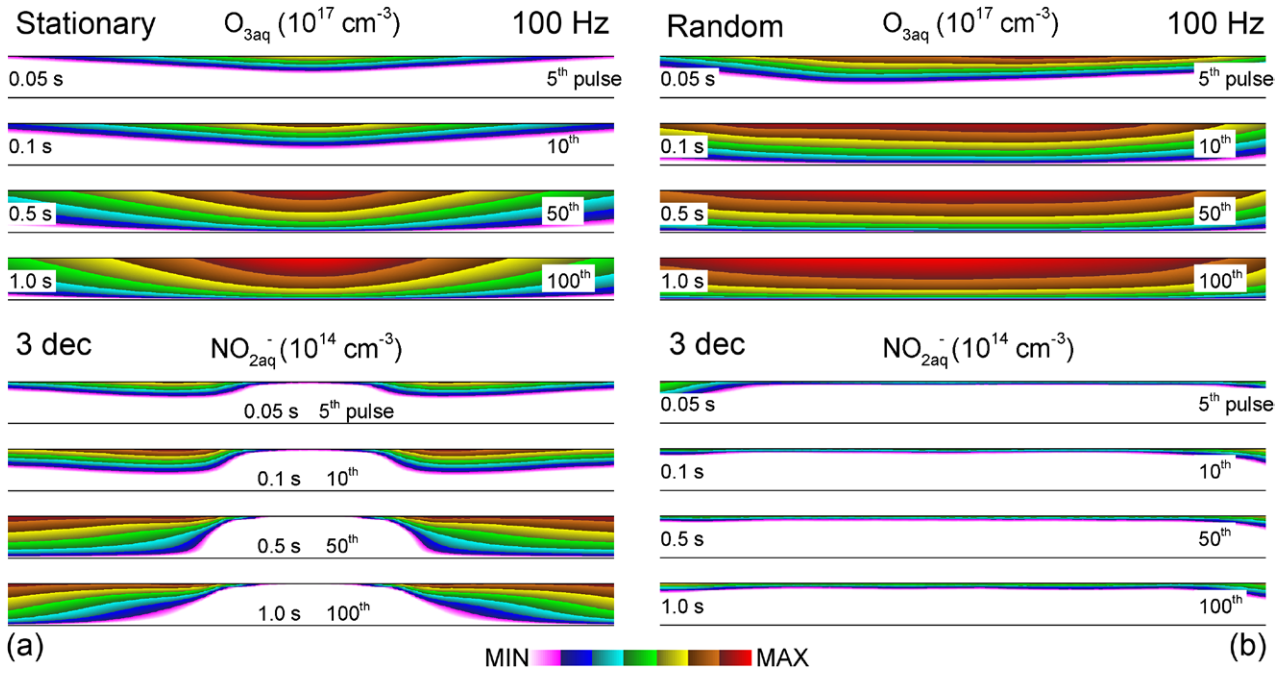

Figure 6. The time evolution of O_{3aq} and NO_{2aq}^- densities in the 200 μm water layer at the end of the 5th, 10th, 50th and 100th pulse for (a) stationary streamers and (b) randomly striking streamers. The time and pulse number are shown in each frame. The contours are plotted on a three-decade log-scale with the maximum values at the top.

is also now uniformly distributed. This consumption of OH_{aq} then decreases the formation of H_2O_{2aq}.

The evolution of O_{3aq} and NO_{2aq}^- is quite similar to that of H_2O_{2aq} and NO_{aq}, and is shown in figure 6. With stationary streamers, the density of O_{3aq} peaks at the center where the source of O_3 and O produced in the streamer is maximum. Recall that the rate of solvation O_3 is slow compared to OH_{aq}, but rapid when compared to NO. So the center peak of gas phase O_3 reflects diffusion away from the centered streamer where O quickly reacts with O_2. O_{3aq} is dominantly produced through solvation of O_3, with less than 2% of its production in the liquid layer being due to reactions of O_{aq} with O_{2aq}. After 100 pulses, the peak density of O_{3aq} is as high as 5×10^{17} cm^{-3} in the middle of the liquid.

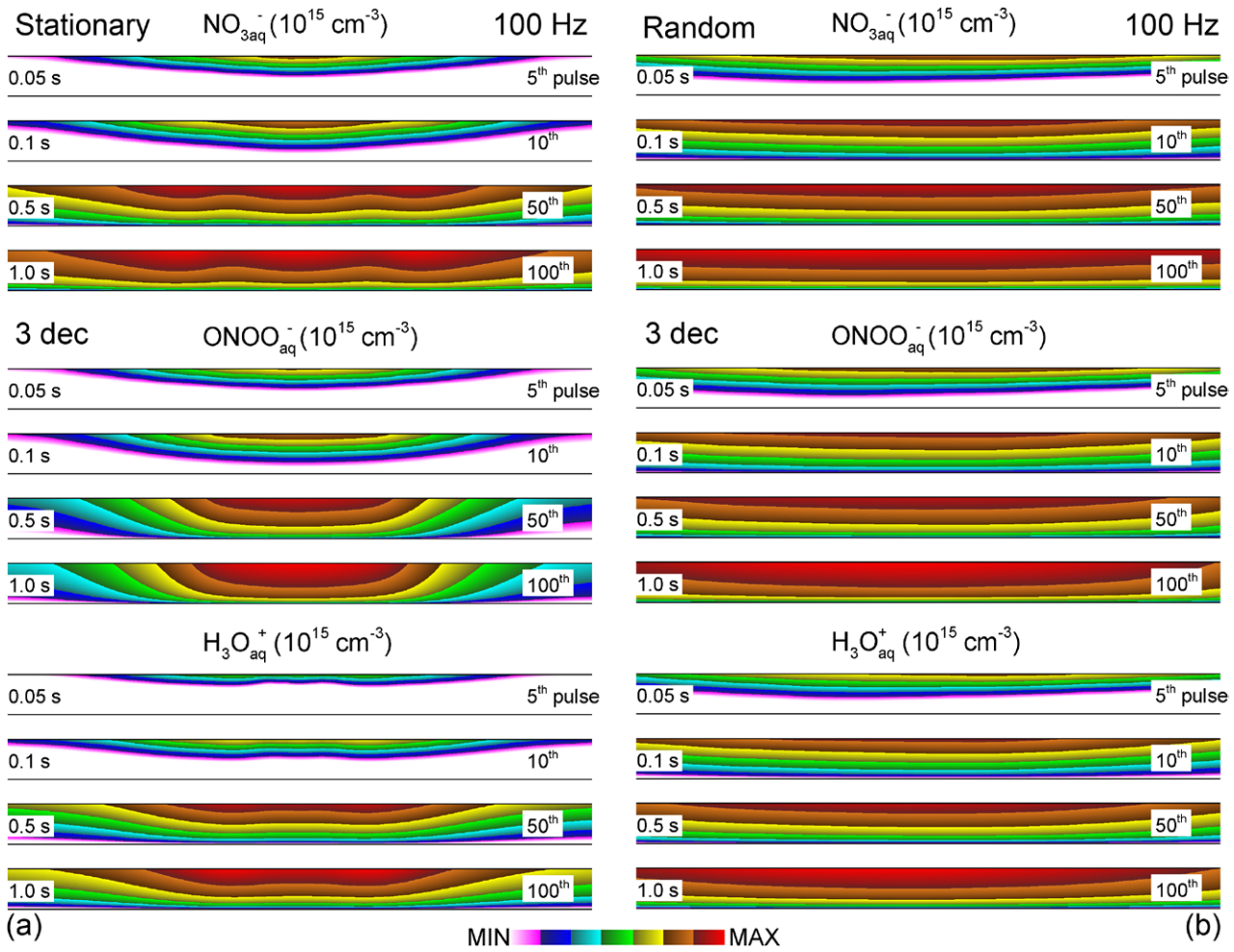

Figure 7. The time evolution of NO_{3aq}^-, $ONOO_{aq}^-$ and $H_3O_{aq}^+$ densities in the 200 μm water layer at the end of the 5th, 10th, 50th and 100th pulse for the randomly striking streamer. The time and pulse number are shown in each frame. The contours are plotted on a three-decade log-scale with the maximum values at the top.

The spatial distribution of NO_{2aq}^-, having a maximum density of 10^{14} cm^{-3}, mirrors that of NO_{aq}. Similar to NO_{aq}, NO_{2aq}^- reacts with OH_{aq} to make NO_{3aq}^-, and so its density is depleted in the center where OH_{aq} is produced—its density accumulates elsewhere. NO_{2aq}^- is also oxidized by O_{3aq} with a lower rate coefficient, which contributes to its depletion near the center where O_{3aq} is higher. OH_{aq} is depleted approaching the underlying tissue and so it is not important to the consumption of NO_{2aq}^- away from the surface. However, NO_{2aq}^- is consumed by reactions with O_{3aq} through the entire depth of the liquid, which results in a wider region of depletion of NO_{2aq}^-. At the side of the domain many streamer radii away from the center, the density of O_{3aq} decreases to below 10^{16} cm^{-3} and NO_{2aq}^- is able to transport through the liquid layer after 0.5 s. However, NO_{2aq}^- is still depleted at a finite rate by reaction with O_{3aq}. At 1.0 s the density of NO_{2aq}^- near the tissue is smaller than that at 0.5 s since by this time O_{3aq} has also reached the underlying tissue. The density of O_{3aq} is much higher than that of NO_{2aq}^-, and so its density is not significantly affected by these reactions.

The evolution of O_{3aq} and NO_{2aq}^- for randomly striking streamers is shown in figure 6(b). O_{3aq} now has fairly uniform distributions in the liquid. For similar reasons as for OH_{aq} and H_2O_{2aq}, these uniform profiles result from the cumulative average of the discretely local contributions of individual streamers. The liquid layer becomes O_{3aq} rich after 100 pulses with a density of 10^{17} cm^{-3} at the top surface. Since NO_{2aq}^- is consumed by OH_{aq} and O_{3aq}, NO_{2aq}^- only appears at the liquid surface with a density of 10^{14} cm^{-3} and does not diffuse deeper into the liquid. Much like NO_{aq}, the NO_{2aq}^- is blocked from reaching the tissue by the now uniform distribution of its oxidizing agents.

The aqueous RNS reactivity represented by the solvation of N_xO_y, which is 90% NO, does not disappear with the reaction with OH_{aq}—it is converted into a different species. For example, the terminal species, NO_{3aq}^- and $ONOO_{aq}^-$, produced by OH_{aq} reacting with nitrogen oxides (N_xO_{yaq}) are shown in figure 7(a) for the stationary striking streamer. Before 10 pulses, the density of NO_{3aq}^- peaks at the center at 3×10^{14} cm^{-3}. After 50 pulses, three regions with concentrations of

10^{15} cm^{-3} appear. The center region of high concentration is due to reaction of the centrally produced OH_{aq} with NO_{aq}. This reaction generates HNO_{2aq}, which hydrolyzes to form its conjugate ion, NO_{2aq}^-. HNO_{2aq} is a weak acid and only 1–3% of HNO_{2aq} will hydrolyze to NO_{2aq}^- [56]. Usually, NO_{2aq}^- is fairly stable in water. However, in the presence of O_{3aq}, NO_{2aq}^- is oxidized to NO_{3aq}^-. This process also ends in the conversion of HNO_{2aq} to NO_{3aq}^-, since hydrolysis of HNO_{2aq} cannot be in equilibrium due to the loss of NO_{2aq}^-. HNO_{3aq} and its conjugate ion, NO_{3aq}^-, are the dominant acid and negative ion in liquid. HNO_{3aq} is a strong acid and almost completely hydrolyzes. The peaks of NO_{3aq}^-, appearing off center result from the solvation and diffusion of NO_{aq} outside of where the streamer strikes. NO_{aq} then slowly produces HNO_{3aq} and NO_{3aq}^- by reaction with water.

Different from NO_{3aq}^-, the distribution of $ONOO_{aq}^-$ is peaked at the center where OH_{aq} is formed by the stationary streamer. Since $ONOOH_{aq}$ and its conjugate ion, $ONOO_{aq}^-$, are dominantly produced through OH_{aq} related reactions, the source of $ONOO_{aq}^-$ reflects the location where OH_{aq} is formed and quickly depleted. The peak density of $ONOO_{aq}^-$ grows from 10^{14} cm^{-3} after the 5th pulse to 1.2×10^{15} cm^{-3} after the 100th pulse. $ONOOH_{aq}$ and its conjugate ion, $ONOO_{aq}^-$, are reactive species which are believed to play an important role in plasma treatment of biological tissues since they have high oxidizing power [58]. These species have been experimentally detected in plasma treated water [59]. In our model, the density of $ONOO_{aq}^-$ may be overestimated. A large density of OH_{aq} and NO_{2aq} make it possible to produce significant amounts of $ONOOH_{aq}$, which soon hydrolyzes to $ONOO_{aq}^-$. Although $ONOOH_{aq}$ is not as strong an acid as HNO_{3aq}, it still rapidly hydrolyzes and in our model $ONOOH_{aq}$ nearly completely hydrolyzes. In deionized water, $ONOO_{aq}^-$ will eventually naturally convert to NO_{3aq}^-. The characteristic time for conversation is believed to be as short as a few seconds [60]. In our model, the conversion time is about 10 s. If the shorter conversion time is the actual case, we may overestimate the production and transport of $ONOO_{aq}^-$, and underestimate that for NO_{3aq}^-.

Superoxide anion, O_{2aq}^-, is also an important oxidant, which can induce oxidative stress in cells. It is experimentally observed in plasma activated water and growth media [57]. In our reaction mechanism, O_{2aq}^- can be formed by reaction of dissolved O_2 with solvated electrons, and for that reason O_{2aq}^- should have a reasonably large density. However, in DBD discharges in air which produce significant amount of NO_{aq}, O_{2aq}^- is depleted by reactions with NO_{aq} to form peroxynitrite, $ONOO_{aq}^-$. In the absence of NO_{aq}, as occurring under the stationary streamer, O_{2aq}^- charge exchanges to OH_{aq}^- by reacting with residual OH_{aq}. Even though OH_{aq} quickly reacts, its depleted density of 5×10^{11} cm^{-3} is still large compared to O_{2aq}^- having a density of 10^{11} cm^{-3}.

The density of hydronium, $H_3O_{aq}^+$, which dominates the positive ions in the liquid, is shown in figure 7(a) for stationary striking streamers. The spatial distribution of $H_3O_{aq}^+$ follows the profiles of the major negative ions NO_{3aq}^- and $ONOO_{aq}^-$ since charge neutrality is maintained in the liquid layer. The density of $H_3O_{aq}^+$ is up to 2×10^{15} cm^{-3} at the center of the layer. Charge exchange by incident positive gas phase ions with water molecules during the discharge pulse (followed by charged exchange of $H_2O_{aq}^+$) dominantly occurs under the streamer and accounts for about 11% of $H_3O_{aq}^+$ production. The remaining 89% occurs through hydrolysis of HNO_{2aq}, HNO_{3aq} and $HOONO_{aq}$ during the interpulse period over a wider area. The production of HNO_{2aq}, HNO_{3aq} and $HOONO_{aq}$ trace their origins to plasma produced N_xO_y, which slowly solvates during the interpulse period. $H_3O_{aq}^+$ acidifies the liquid and increases its conductivity, which will be discussed later.

The evolution of the densities of NO_{3aq}^-, $ONOO_{aq}^-$ and $H_3O_{aq}^+$ with randomly striking streamers is shown in figure 7(b). The production channels of these species are the same as discussed for the stationary streamer. As a result of uniformly mixing OH_{aq} and NO_{aq} by the randomly striking streamers, the densities of NO_{3aq}^- and $ONOO_{aq}^-$ are quite uniform compared to the stationary scheme. Since OH_{aq} reacts with nitrogen oxides, $ONOO_{aq}^-$ has a higher density, 10^{15} cm^{-3} across the entire surface after 100 pulses compared to the stationary streamer. NO_{3aq}^- also has a uniform profile with a density of 9×10^{14} cm^{-3}, which is slightly lower than $ONOO_{aq}^-$. The distribution of $H_3O_{aq}^+$ is fairly uniform as well, following the profile of NO_{3aq}^- and $ONOO_{aq}^-$.

The volume average densities of solvated species are shown in figure 8, for stationary and randomly striking streamers. Since the DBD is operated in air, significant amounts of O_3 are produced in the gas phase which then solvate into the liquid layer. The average density of O_{3aq} increases with the number of pulses and is nearly independent of the pulse scheme, stationary or random. At the end of 100 pulses, the average density of O_{3aq} reaches 10^{17} cm^{-3}. HNO_{2aq} and its conjugate ion, NO_{2aq}^-, are slowly converted in ozone-rich liquid to HNO_{3aq} and its conjugate ion, NO_{3aq}^-. Otherwise, a significant density of HNO_{2aq} and NO_{2aq}^- would be formed. For example, in He or Ar discharges in contact with water, O_3 production is much reduced and HNO_{2aq} and NO_{2aq}^- are found to be terminal species [56, 57]. H_{aq} and H_{2aq} are also oxidized by O_{3aq} in the liquid to produce OH_{aq} and then H_2O_{2aq}. The density of H_2O_{2aq} is therefore increased in ozone-reach environments. With a stationary streamer, the densities of H_2O_{2aq} and NO_{aq} monotonically increase, resulting from the separation in space of OH_{aq} and NO_{aq}, as shown in figure 5. After 100 pulses, the average densities of H_2O_{2aq} and NO_{aq} reach 5×10^{14} cm^{-3} and 4×10^{14} cm^{-3}. H_2O_{2aq} is a terminal species with its only major loss being to the underlying tissue. NO_{aq} slowly reacts with water and can last for 10 s. With pulses occurring at 100 Hz, the production of H_2O_{2aq} is greater than its rate of diffusion loss to the underlying tissue. As a result, the density of H_2O_{2aq} increases with the number of pulses. At lower frequencies with a longer interpulse period, the loss of H_2O_{2aq} to the underlying tissue between pulses would produce lower average densities.

With randomly striking streamers, OH_{aq} and NO_{aq} are well mixed and react throughout the liquid. NO_{aq} therefore does not accumulate and reaches a density of only 10^{12} cm^{-3} after 100 pulses. H_2O_{2aq} rises to 2×10^{14} cm^{-3} after about 13 pulses and then decreases. The peak is due to the slowly solvating NO from the gas phase. Prior to NO solvating into the liquid, H_2O_{2aq} accumulates by self-reactions of OH_{aq}. After NO begins to solvate into the liquid, OH_{aq} is consumed by reaction with NO_{aq}, which then reduces the production of H_2O_{2aq}. This is a significant difference compared to the stationary streamer in which H_2O_{2aq} is formed under the streamer where NO_{aq} is depleted. The density of H_2O_{2aq} decreases below 1.6×10^{14} cm^{-3} after 100 pulses since consumption OH_{aq} by NO_{aq} surpasses its loss in the formation of H_2O_{2aq}. For these conditions, the density of H_2O_{2aq} will not increase by increasing the number of pulses. In order to produce more H_2O_{2aq} in liquid, a cross flow (>270 sccm for a 100 Hz DBD) through the gas gap might be necessary to blow away NO before it solvates. OH_{aq} would then be less consumed by reactions with NO_{aq}, resulting in more production of H_2O_{2a}.

The average densities of the ions $H_3O^+_{aq}$, NO^-_{3aq} and $ONOO^-_{aq}$ are shown in figure 8(c). These densities monotonically increase with both stationary and randomly striking streamers. $H_3O^+_{aq}$ reaches a density of 9×10^{14} cm^{-3} after 100 pulses in the random scheme. Although charge exchange of $H_2O^+_{aq}$ with water molecules produces $H_3O^+_{aq}$, the hydrolysis of acids, such as HNO_{3aq} and $HOONO_{aq}$, dominates the production of $H_3O^+_{aq}$ in the long term. Therefore, the density of $H_3O^+_{aq}$ nearly equates to about the sum of NO^-_{3aq} and $ONOO^-_{aq}$. With randomly striking streamers, OH_{aq} and N_xO_{yaq} are well mixed, and more $HOONO_{aq}$ is produced than HNO_{3aq}, which then results in larger densities of $ONOO^-_{aq}$ compared to NO^-_{3aq}. In the stationary scheme, the production channels for ions are similar. However, since OH_{aq} is spatially separated from N_xO_{yaq}, the production of the precursors to hydrolysis are significantly reduced, which then reduces the production of $H_3O^+_{aq}$, NO^-_{3aq} and $ONOO^-_{aq}$. In general, the average densities of ions are lower with stationary streamers by a factor of ≈2.

What ultimately matters to the treatment of the tissue are the fluences of reactive species to its surface. These fluences are shown in figure 9. There is significant spatial variation in the fluences for the discharges that have stationary streamers, and significant differences in which species reach the tissue between the stationary and random schemes. With stationary streamers, the tissue can receive a significant fluence of NO_{aq}, while the tissue receives virtually no NO_{aq} with randomly striking streamers. In the stationary scheme, the fluence of NO_{aq} to the tissue is a minimum under the streamer and maximum many radii away due to the diffusion of NO_{aq} around the location that the streamer strikes the liquid. In contrast, the fluence of H_2O_{2aq} is maximum under the streamer, decreasing from 10^{15} cm^{-2} at the center to $<10^{12}$ cm^{-2} less than 1 mm away. These trends could result in an overdose of H_2O_{2aq} under the streamer and underdose elsewhere. In the random scheme, the fluence of H_2O_{2aq} is uniform, but with a

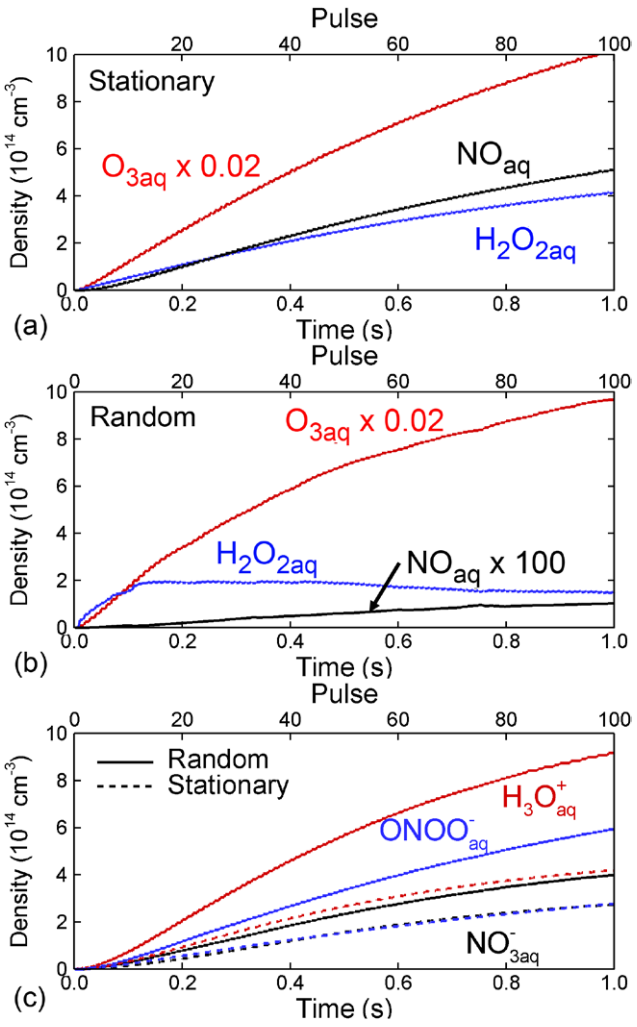

Figure 8. The time evolution of densities averaged in the liquid layer over 100 pulses for neutral species with (a) stationary and (b) random streamers, and for (c) charged species for both schemes. The O_{3aq} density is reduced by a factor of 50 and that of NO_{aq} is increased by a factor of 100. The time and corresponding pulse number are shown at the bottom and top axes.

lower value of 2×10^{12} cm^{-2} due to the uniform consumption of its precursor OH_{aq}. The fluence of O_{3aq} also has a peak value, 2×10^{15} cm^{-2}, at the center and decreases to 2×10^{14} cm^{-2} to the edge in the stationary scheme. In the random scheme, the fluence of O_{3aq} is quite uniform with a value around 10^{15} cm^{-2}.

The trends for the fluences of neutral species are reflected in the fluences of charged species. With stationary streamers, the fluence of $ONOO^-_{aq}$ basically follows that of H_2O_{2aq}, since $ONOO^-_{aq}$ is produced in large part from reactions related to OH_{aq}. At the center, the fluence of $ONOO^-_{aq}$ is 3×10^{13} cm^{-2} and decreases to $<10^{12}$ cm^{-2} a mm away. The fluence of NO^-_{3aq} is fairly uniform since it is produced through N_xO_{yaq} reacting with water. The local maxima in the fluence of NO^-_{3aq} reflect the interaction of OH_{aq} and NO_{aq} at the interface where the density of OH_{aq} is large in the center and the density of NO_{aq} is large in the periphery. $H_3O^+_{aq}$ is basically given by the

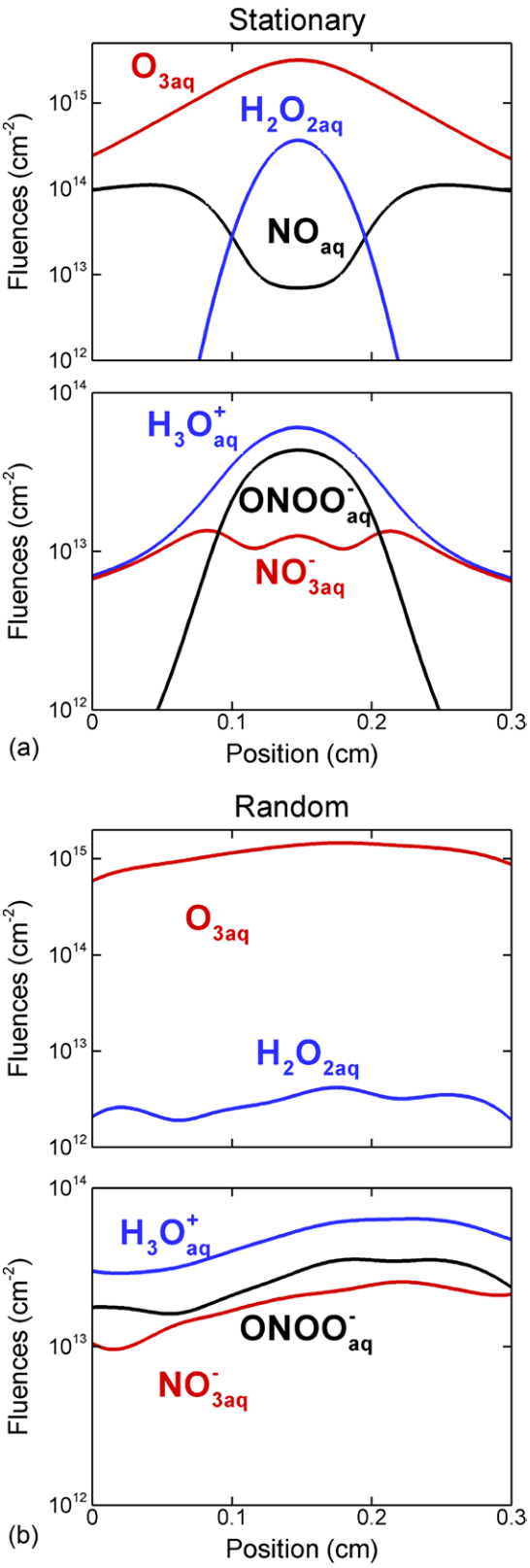

Figure 9. Fluences of neutral and charged species integrated over 100 pulses and a 10 s afterglow onto the tissue underlying the 200 μm water layer. (a) Stationary pulses and (b) randomly striking pulses.

sum of negative ions, dominated by NO^-_{3aq} and $ONOO^-_{aq}$, and so the fluence of $H_3O^+_{aq}$ also reflects the peak of $ONOO^-_{aq}$ and the broader distribution of NO^-_{3aq}.

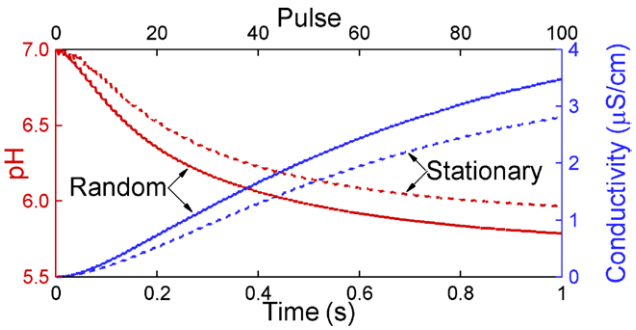

Figure 10. The time evolution of average pH and conductivity of the liquid layer over 100 discharge pulses in the stationary and random schemes. The time axis and corresponding pulse number are shown at the bottom and top.

With randomly striking streamers, the fluences of ions become more uniform. The fluence of $ONOO^-_{aq}$ is higher than in the stationary scheme since nitrogen oxides and OH_{aq} are well mixed. As expected, the fluences of reactive species are more uniform with randomly striking streamers which could result in higher quality treatment in plasma medicine applications. However, for example, if NO_{aq} is a desired agent for treatment, only the stationary scheme can produce significant fluences of NO_{aq} to the tissue.

One of the consequences of long-term DBD treatment is altering the characteristics of the liquid layer. As discussed above, after 100 pulses the liquid becomes O_{3aq} rich, decreasing the ability to produce large densities of HNO_{2aq} and NO^-_{2aq}. Another effect is that the liquid layer becomes acidified and conductive, as shown in figure 10. After 100 pulses, the pH decreases to 6 for stationary streamers and 5.8 for randomly striking streamers. The pH value calculated in our model is determined by the density of hydronium, $H_3O^+_{aq}$, in which we assumed all hydronium ions to be reactive. These pH values can be considered an upper limit as the consumption of species by the tissue reduces the densities of $H_3O^+_{aq}$ and results in a higher pH value than might otherwise be produced.

In experiments by Hamaguchi *et al* [12], pH values of a plasma jet treated aqueous solution were evaluated from hydronium concentrations, which were assumed to be equal to that of the measured NO^-_{xaq} ($x = 2$, 3) ions. The estimated pH values from the NO^-_{xaq} concentration were in good agreement with those directly measured by a pH meter. The pH decreased to 4.5 after 3 min of plasma treatment from an initial value of 5.7. In another indirect surface DBD treatment [13], the pH decreased from 7 to less than 4 in non-buffered physiological saline within the first 5 min of plasma treatment, followed by a slower decrease to between 2 and 3 in 30 min. Reduction of pH value or acidification of liquid is known to affect the viability of bacteria through either directly interacting or assisting other reactive species. Our predicted values of pH extrapolate to 4.8 after 100 s plasma treatment with 10 000 pulses. Considering that only a single streamer is modeled in this computational investigation, the acidification is already significant.

The predicted conductivity of the liquid after 100 pulses, also shown in figure 10, increases to 2.8 μS cm^{-1} for

stationary streamers and 3.5 μS cm^{-1} for randomly striking streamers. (The conductivity in our model is determined by the total ion density in the liquid with collision cross sections approximated by Lennard-Jones potentials.) This value is likely a lower limit due to the consumption of ions on the tissue. Extrapolating these results to 5 min of treatment and 30 000 pulses, the predicted conductivity is 1 mS cm^{-1}. For comparison, in a DC discharge with deionized liquid as the cathode [11], the liquid conductivity was observed to increase to 30 μS cm^{-1} after a 10 min treatment and by 150 μS cm^{-1} after a 1 h treatment. High quality deionized water has a conductivity of about 0.1 μS cm^{-1} and the conductivity of typical tap water is in the range of 100–1000 μS cm^{-1}. Therefore, the conductivity of deionized water is altered within seconds of treatment, whereas significant treatment (many minutes or more) is required to affect the conductivity of tap water.

The effects of the conductivity of the liquid on discharge properties can be complex. One such effect results from the reduced voltage drop in the liquid due to its higher conductivity. This in turn increases the voltage drop in the gas above the liquid. For example, an otherwise identical discharge was modeled with pre-dissolved NaCl in the liquid giving a conductivity of 1 mS cm^{-1}. The electric field in the gas gap was enhanced by the reduced voltage drop in the liquid and the accumulation of surface charges from polarization of the conductive liquid. The electron density in the plasma streamer increased by a factor of two compared to a streamer over an initially non-conducting liquid. The plasma streamer spread over a wider area and so delivered plasma produced species (e.g. ions, rapidly solvating neutrals, photons) over this broader area. For conditions where the conductivity of the liquid approaches 1 mS cm^{-1}, our assumption that each discharge pulse is identical is no longer valid.

We discussed that NO_{aq} and NO_{2aq}^- are consumed by reactions with OH_{aq} and O_{3aq}, and so conditions for which there is an abundance of OH_{aq} and O_{3aq} in spatial coincidence with NO_{aq} and NO_{2aq}^- will reduce their densities. Considering the possible biomedical effects produced by NO_{aq} and NO_{2aq}^-, it may be desirable to control the densities and fluences of these species to the tissue by controlling the coincidence of NO_{aq} and NO_{2aq}^- with OH_{aq} and O_{3aq}. One such method is to change the repetition rate of the discharge. The densities of H_2O_{2aq}, NO_{aq} and NO_{2aq}^- produced by a 10 Hz DBD with a stationary streamer are shown in figure 11 at 1 μs after discharge pulses. In a 10 Hz DBD, the interpulse period is 0.1 s, which is long enough for transport of aqueous species significantly through the liquid layer. So at 10 Hz, species produced on a prior pulse are able to diffuse away from the surface before species produced by the next pulse solvate into the liquid. For example, due to the longer interpulse period, H_2O_{2aq} diffuses to a wider distribution having a lower density compared to the 100 Hz case where H_2O_{2aq} accumulates on a pulse-to-pulse basis.

The density of NO_{aq} demonstrates these repetition rate dependent dynamics. NO uniformly solvates into the liquid throughout the interpulse period. OH_{aq} is produced under the streamer coincident with each discharge pulse. This surface resident OH_{aq} depletes NO_{aq} at the center of the liquid layer.

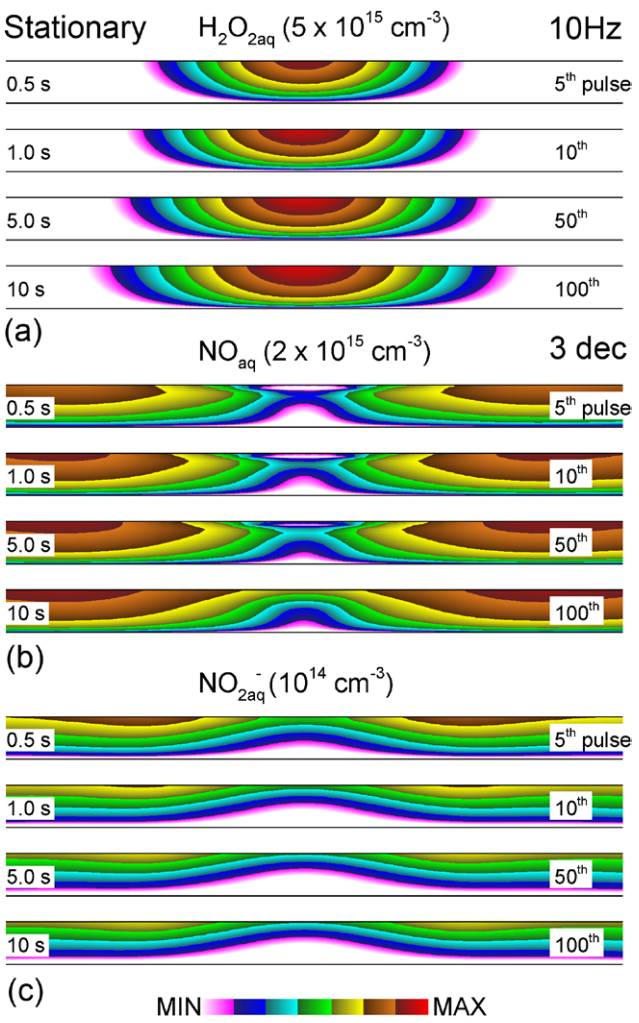

Figure 11. The densities of (a) H_2O_{2aq}, (b) NO_{aq} and (c) NO_{2aq}^- in the 200 μm water layer during 10 Hz DBD treatment for the stationary streamer. The densities are shown accumulating after the 5th, 10th, 50th and 100th pulse. The time and corresponding pulse number are shown in each frame. The contours are plotted on a three-decade log-scale with the maximum values at the top.

Due to the reactivity of OH_{aq}, it does not penetrate far beyond the surface and does not survive for longer than 0.6 ms. At 10 Hz, the interpulse period is long enough so that NO_{aq} is able to diffuse into the center of the liquid layer where OH_{aq} is depleted. At the higher 100 Hz repetition rate, NO_{aq} is consumed by the replenished OH_{aq} produced by the next pulse before NO_{aq} can reach the center of the layer. The separation of NO_{aq} and OH_{aq} both in space and time due to the longer interpulse period results in a significant amount of NO_{aq} reaching the tissue at the center of the layer.

The coincidence (or lack thereof) of species afforded by the 10 Hz PRF also affects the density of NO_{2aq}^-. With the longer interpulse period, NO_{2aq}^- can diffuse deeper into the liquid layer and almost reach the underlying tissue. The density of NO_{2aq}^- increases to 10^{14} cm^{-3} within 10 pulses before decreasing to 10^{13} cm^{-3} after the following 90 pulses. During the initial pulses, NO_{2aq}^- is produced in a nearly pristine water layer and with the longer interpulse period reaches the tissue.

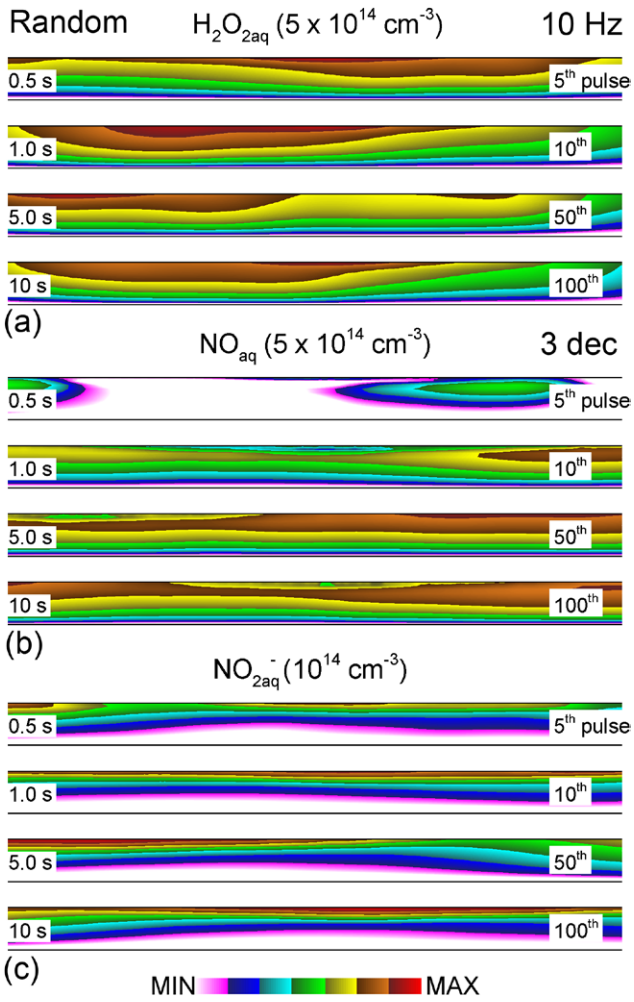

Figure 12. The densities of (a) H_2O_{2aq}, (b) NO_{aq} and (c) NO_{2aq}^- in the 200 μm water layer during 10 Hz DBD treatment for the randomly striking streamer. The densities are shown accumulating after the 5th, 10th, 50th and 100th pulse. The time and corresponding pulse number are shown in each frame. The contours are plotted on a three-decade log-scale with the maximum values at the top.

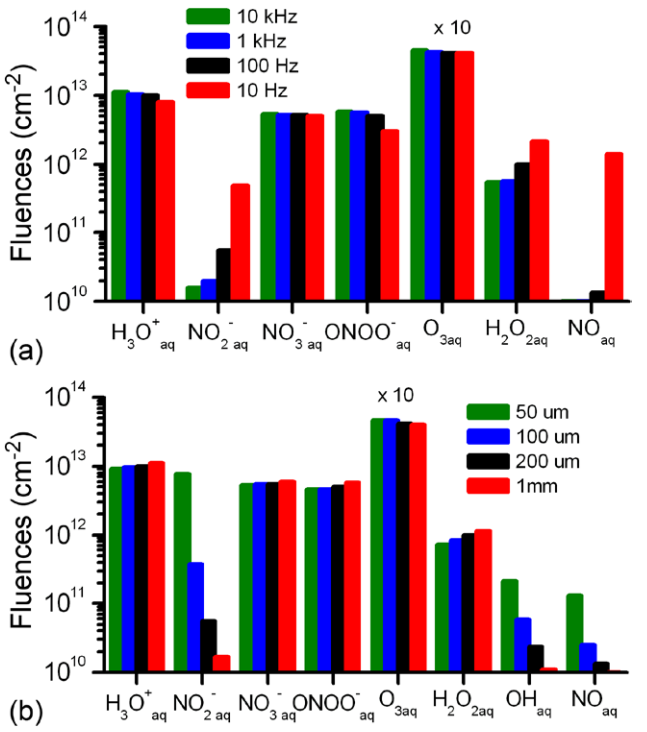

Figure 13. Integrated fluences of reactive species over 10 s onto the underlying tissue. (a) Fluences for pulse repetition frequencies of 10 Hz to 10 kHz for a 200 μm liquid layer. (b) Fluences for a 100 Hz DBD with liquid thickness varying from 50 μm to 1 mm. The fluence of O_{3aq} is reduced by a factor of 10.

However, after tens of pulses, the increasing density of O_{3aq} consumes NO_{2aq}^-, thereby decreasing its flux to the tissue.

The densities of H_2O_{2aq}, NO_{aq} and NO_{2aq}^- produced by 10 Hz DBDs with randomly striking streamers are shown in figure 12. The density of H_2O_{2aq} is lower by a factor of two than that produced in 100 Hz DBDs due to the loss of H_2O_{2aq} to the underlying tissue during the interpulse period. The profile of H_2O_{2aq} always has a peak where the previous plasma streamer strikes due to the impulsive production of H_2O_{2aq} by the rapid (but isolated in time) injection of OH_{aq}. The interpulse period is long enough at 10 Hz that NO_{aq} is able to diffuse away from the surface before the next pulse produces the surface resident OH_{aq}. Since the discharge pulses randomly strike the surface of the liquid, the NO_{aq} may have many interpulse periods to diffuse away from the surface before another streamer strikes close enough to produce additional OH_{aq} that would reduce the density NO_{aq}. In the 100 Hz discharge, the NO_{aq} is not able to diffuse away from the surface before another discharge produces OH_{aq} that consumes it. For example, NO_{aq} appears at two locations in the bulk liquid layer after five pulses. These are regions where, statistically, NO_{aq} was able to diffuse away from the surface prior to a subsequent discharge pulse producing OH_{aq} at the surface. After 10 pulses, this statistical *escape* of NO_{aq} from the surface results in its accumulation of NO_{aq} in the bulk liquid to a density of 10^{14} cm^{-3}. After 50 and 100 pulses, NO_{aq} accumulates uniformly to 5×10^{14} cm^{-3}, while its distribution shows isolated regions near the surface where a recent streamer striking the liquid produced OH_{aq} that locally consumed NO_{aq}. Compared to 100 Hz PRFs, the longer interpulse period in 10 Hz DBDs enables NO_{aq} to survive diffusing through the liquid layer and reach the underlying tissue.

Similar to NO_{aq}, in the 10 Hz DBD with the longer interpulse period, NO_{2aq}^- is able to diffuse into the bulk liquid layer instead of being consumed by OH_{aq} at the liquid surface. However, NO_{2aq}^- is still not able to diffuse entirely through the liquid layer due to its consumption by O_{3aq}. Although not shown here, due to its lower reactivity in the liquid, O_{3aq} still fills the liquid layer at the lower PRF with densities as high as 5×10^{16} cm^{-3}. In the ozone-rich liquid layer, NO_{2aq}^- is slowly converted to NO_{3aq}^-. The interpulse period of 0.1 s is just long enough for this slow process, resulting in NO_{2aq}^- being converted to NO_{3aq}^- by O_{3aq} just before it reaches the underlying tissue. To be clear, a small amount of NO_{2aq}^- does reach the underlying tissue since the conversion process is not complete.

Reducing the pulse frequency from 100 Hz to 10 Hz results in NO_{aq} being able to diffuse through the liquid to reach the underlying tissue. This suggests that the fluences of some

species to the underlying tissue can be controlled by varying the PRF. Fluences of reactants to the tissue are shown in figure 13(a) for PRFs of 10 Hz to 10 kHz with randomly striking streamers. In each case, 100 pulses are computed followed by 10–60 s of afterglow. The fluence of NO_{aq} to the tissue is negligible for 10 kHz and 1 kHz as the production of OH_{aq} at the surface is frequent enough to prevent the *escape* of NO_{aq} into the bulk liquid. The fluence of NO_{aq} increases to 1.5×10^{10} cm^{-2} for 100 Hz and sharply increases to 1.9×10^{12} cm^{-2} for 10 Hz. Similarly, the fluence of NO^-_{2aq} increases from 1.8×10^{10} cm^{-2} for 10 kHz to 4.5×10^{11} cm^{-2} for 10 Hz. The fluence of H_2O_{2aq} also increases by a factor of three from higher frequency to lower frequency. This increase in H_2O_{2aq} results from less NO_{aq} reacting with OH_{aq}, which is the source of H_2O_{2aq}. For the same reason the fluence of $ONOO^-_{aq}$ decreases with lower frequency since $ONOO^-_{aq}$ is produced by reaction between NO_{aq} and OH_{aq}. The fluence of $H_3O^+_{aq}$ has a small decrease at low frequency following the decrease in $ONOO^-_{aq}$. The fluences of NO^-_{3aq} and O_{3aq} are not particularly sensitive to PRF since their fluences are determined by the rate of solvation of gas phase species averaged over pulses.

The sensitivity of fluences to PRF results from an accumulation effect, diffusion processes and reactions between long-lived and short-lived species. Accumulation of long-lived species, like O_{3aq}, is able to alter the characteristics of the liquid layer. Diffusion away from the surface reduces the coincidence of reactants, as is the case for NO_{aq} being consumed by OH_{aq} at the liquid surface. However, lack of coincidence between NO_{aq} and OH_{aq} may reduce production $HOONO_{aq}$, which is an important oxidizing agent in medical treatment. Lower frequencies and longer interpulse periods reduce the interactions between pulses of short-lived species whereas interactions with longer-lived species such as O_{3aq} are less sensitive to PRF. The interactions between pulses also occur in the gas phase. Higher PRFs results in accumulation of reactants that favor formation of species requiring many reactions, such as N_xO_y [49].

In addition to frequency, the thickness of the liquid layer also affects the fluences of species. For example, for the randomly striking streamers, NO_{aq} has a significant density only at the liquid surface, as shown in figure 5(b). This implies that the underlying tissue can still receive a large fluence of NO_{aq} if the liquid layer is thin enough. Fluences of reactive species onto the underlying tissue with randomly striking streamers are shown in figure 13(b) for different thickness of the liquid layer while keeping the air gap height the same. The fluence of NO_{aq} increases from 10^{10} cm^{-2} with a 1 mm liquid layer to 10^{11} cm^{-2} with 50 μm liquid layer. The fluence of NO^-_{2aq} increases from 10^{10} cm^{-2} with 1 mm liquid layer to 10^{13} cm^{-2} with 50 μm. The thin liquid layer enables more NO^-_{2aq} to reach the tissue before being consumed by O_{3aq}. OH_{aq} is also able to reach the tissue for a thin liquid layer of 50 μm with a fluence of 2×10^{11} cm^{-2}. For a thick liquid layer of 1 mm the fluence of OH_{aq} is reduced to 10^{10} cm^{-2}. The corresponding fluence of H_2O_{2aq} increases a small amount with the thickness of the liquid layer since more OH_{aq} converts to H_2O_{2aq} instead of being lost to the tissue. The fluences of $H_3O^+_{aq}$, NO^-_{3aq}, $ONOO^-_{aq}$ and O_{3aq} are not sensitive to the thickness of the liquid layer. The characteristic time for species to diffuse through the liquid layer increases proportionally with the square of the thickness of the liquid layer. From 50 μm to 1 mm, the characteristic time for diffusion through the liquid increases by a factor of 400. This difference in diffusion time enables short-lived species like OH_{aq}, NO_{aq} and NO^-_{2aq} to reach the surface. Thinner liquid layers tend to increase the fluences of short-lived species, while thicker liquid layers tend to remove short-lived species. Long-lived species are generally not affected by the thickness for the range we investigated.

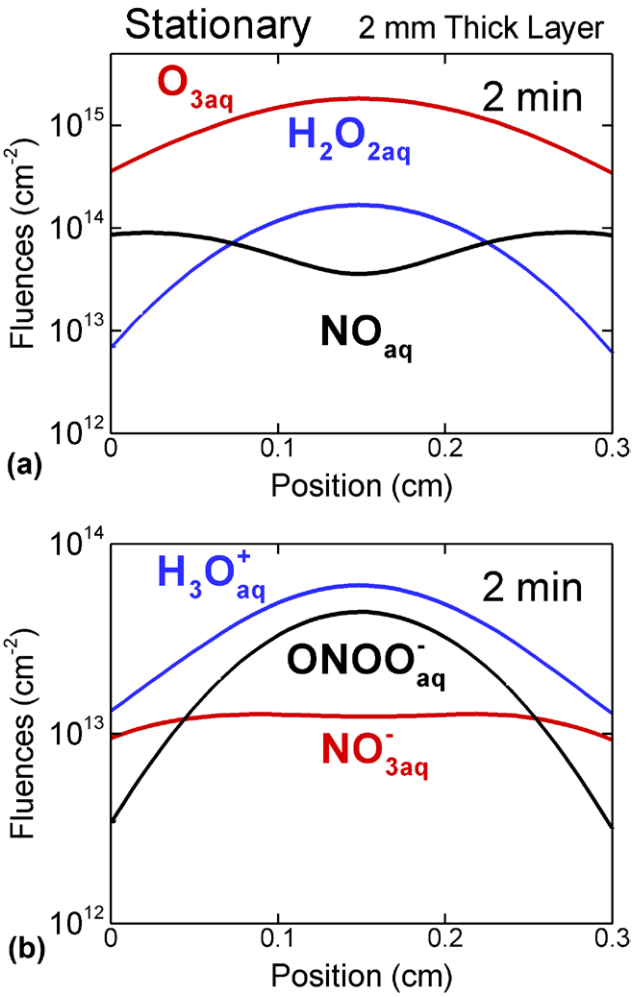

Figure 14. Fluences integrated over 100 pulses and a 2 min afterglow onto the tissue underlying the 2 mm water layer. (a) Neutral and (b) charged species for the stationary streamer.

The spatial distribution of fluences of species with stationary pulses is more sensitive to the thickness of the liquid compared to the randomly striking streamers. In both schemes, the magnitudes of the fluences are sensitive to the transit time, which then discriminate between short- and long-lived species. For example, the fluences of species to the tissue for stationary streamers for a 2 mm thick liquid layer, 100 pulses at 100 Hz, and a 2 min afterglow are shown in figure 14. In general, the fluences in figure 14 are more uniform compared to those for a 200 μm layer as shown in figure 9. The longer

transit time required for a 2 mm layer enables the majority of the reaction chemistry to proceed, converting most reactivity to terminal species. This leaves diffusion to be the dominant process determining the spatial distribution of fluences, a process that tends to make the fluences more uniform. The end result is that some control over both composition and uniformity can be achieved by combinations of repetition rate and thickness of the water layer. For example, for more uniform and larger fluences of NO_{aq}, one should operate at lower PRF and thicker layers. As the layer becomes thicker, the importance of fluid dynamics within the layer increases [61, 62]. In this model, we consider only diffusion within the liquid layers, a simplification enabled by the layers being thin. However, as the layer thickens, convection becomes more important, either natural or forced. With sufficient convection, the *well-stirred* approximation is approached. For example, a *well-stirred*, but still thin water layer would result in mixing OH_{aq} with NO_{aq}. This mixing would result in the uniform consumption of NO_{aq}, and uniform production of nitric acid, and peroxynitrous acid. However, in the case of plasma treating a wound in a clinical or surgical setting, the liquid is usually thin and adheres strongly to the tissue. Significant fluid dynamics within the layer are likely not important. In these cases, the distinctions between stationary and randomly striking streamers, low PRF and high PRF, and thickness are likely still important.

IV. Concluding remarks

The influence of streamer placement, repetition rate and liquid thickness on the fluences of reactive species through thin liquid layers was discussed using results from a computational investigation of DBDs in contact with water overlying tissue. The DBDs were simulated for 100 stationary or randomly striking streamers at different repetition rates in contact with liquid layers of various thicknesses followed by 10 s to 2 min of afterglow. With stationary plasma streamers striking the same location, different rates of solvation of gaseous species produce spatial separation of aqueous species in the liquid. For example, OH with a higher rate of solvation concentrates in both the gas and liquid phase where the plasma streamer strikes. NO with a much lower rate of solvation spreads over the liquid surface. NO_{aq} at the center is nearly completely consumed by $OH_{aq,}$ while NO_{aq} accumulates and reaches the underlying tissue at more distant locations. OH_{aq} is partly constrained to the radius of the plasma streamer due to this reaction with NO_{aq}. With streamers randomly striking the liquid surface, nearly all solvating species are mixed at the surface of the liquid. For example, NO_{aq} is consumed by OH_{aq} over the entire liquid surface and does not reach the underlying tissue for moderate repetition rates. OH_{aq} becomes fairly uniform in liquid.

Even for exposures of only a few seconds the characteristics of the liquid layer can be altered by plasma treatment. The liquid becomes acidic, conductive and ozone-rich after even 100 pulses. An acidic environment enhances the reactivity of species such as peroxynitrite. Nitrous acid and nitrite ions are converted to nitric acid and nitrate ions, respectively, in ozone-rich liquids. The plasma dynamics can also be affected by the conductivity of the liquid layer due to charge separation at the surface and voltage division.

In addition to the spatial locations of the streamers, frequency combined with thickness of the liquid layer is also a method of controlling the plasma produced aqueous species reaching the underlying tissue. Reducing the pulse frequency produces a higher density of short-lived species, such as NO_{aq}, in the liquid. For example, with a 10 Hz DBD, NO_{aq} is able to diffuse from the liquid surface where OH_{aq} is produced during the 0.1 s interpulse and avoids being consumed by the OH_{aq} generated by the next pulse. The NO_{aq} can then reach the underlying tissue. With higher frequencies, the consumption of NO_{aq} by OH_{aq} at the liquid surface is increased.

The transit time for species to the underlying tissue is determined by the thickness of the liquid layer in our model as diffusion in the liquid is the only transport mechanism. Hence, the fluences of short-lived species are sensitive to the thickness of the liquid layer. Short-lived species are able to reach the underlying tissue through a thin liquid layer through which the transit time is short. However, the transit time through a thick liquid layer may be longer than the lifetime of short-lived species, which are eventually depleted before reaching the tissue. As a result, DBDs at lower frequency with a thin liquid layer will result in higher fluences of short-lived species. The thickness of the liquid layer also affects the spatial distribution of fluences to the tissue resulting from stationary pulses. With a 200 μm thick liquid layer, the reactant fluences are non-uniform. For example, the fluence of H_2O_{2aq} peaks at the center where the fluence of NO_{aq} is a minimum. With a 2 mm thick liquid layer, the fluences of H_2O_{2aq} and NO_{aq} become fairly uniform.

Many of these trends strictly apply to thin liquid layers where convection is not important. As the convective component of transport increases and the well-stirred reactor approximation is approached, some of these trends will no longer apply. For example, in the well-stirred limit, NO_{aq} will not have an opportunity to *escape* from the surface where OH_{aq} is formed or to avoid regions of high OH_{aq} afforded by stationary streams. NO_{aq} would then likely be more consumed by OH_{aq}. For the same reasons, more mixing of O_{3aq} with NO^-_{2aq} would produce larger densities of NO^-_{3aq}. The well stirred limit would likely enable more uniform reactions between OH_{aq} and NO_{xaq}, which ultimately will produce a more acidic solution.

Acknowledgments

This work was supported by the Department of Energy Office of Fusion Energy Science (DE-SC0001319) and the National Science Foundation (CHE-1124724).

References

[1] Klämpfl T G, Isbary G, Shimizu T, Li Y-F, Zimmermann J L, Stolz W, Schlegel J, Morfill G E and Schmidt H-U 2012 *Appl. Environ. Microbiol.* **78** 5077
[2] Moisan M *et al* 2013 *Eur. Phys. J. Appl. Phys.* **63** 10001

[3] Isbary G *et al* 2013 *Clin. Plasma Med.* **1** 25
[4] Isbary G *et al* 2012 *Br. J. Dermatol.* **167** 404
[5] Keidar M 2015 *Plasma Source Sci. Technol.* **24** 033001
[6] Tanaka H *et al* 2014 *IEEE Trans. Plasma Sci.* **42** 3760
[7] Pavlovich M J, Chen Z, Sakiyama Y, Clark D S and Graves D B 2013 *Plasma Process. Polym.* **10** 69
[8] Daeschlein G, Scholz S, Ahmedb R, von Woedtke T, Haase H, Niggemeier M, Kindel E, Brandenburg R, Weltmann K-D and Juengera M 2012 *J. Hosp. Infect.* **81** 177
[9] Weltmann K-D, Kindel E, von Woedtke T, Hähnel M, Stieber M and Brandenburg R 2010 *Pure Appl. Chem.* **82** 1223
[10] von Woedtke T, Metelmann H-R and Weltmann K-D 2014 *Contrib. Plasma Phys.* **54** 104
[11] Bruggeman P, Ribezl E, Maslani A, Degroote J, Malesevic A, Rego R, Vierendeels J and Leys C 2008 *Plasma Sources Sci. Technol.* **17** 025012
[12] Ikawa S, Kitano K and Hamaguchi S 2010 *Plasma Process. Polym.* **7** 33
[13] Oehmigen K, Hahnel M, Brandenburg R, Wilke Ch, Weltmann K-D and von Woedtke T 2010 *Plasma Process. Polym.* **7** 250
[14] Garcia M C, Mora M, Foster J E, Gamero A, Sola A, Jiménez-Sanchidrián C, Romero-Salguero F J 2015 Generation of hydrogen peroxide in liquid water using an argon microwave surface wave sustained discharge COST Action TD1208 Electrical Discharges with *L*iquids for Future Application (Barcelona, Spain, February 2015) Paper WG4-1
[15] Traylor M J, Pavlovich M J, Karim S, Hait P, Sakiyama Y, Clark D S and Graves D B 2011 *J. Phys. D: Appl. Phys.* **44** 472001
[16] Tian W and Kushner M J 2014 *J. Phys. D: Appl. Phys.* **47** 165201
[17] Hirst A M, Frame F M, Maitland N J and O'Connell D 2014 *BioMed Res. Int.* **2014** 878319
[18] Alkawareek M Y, Algwari Q T, Gorman S P, Graham W G, O'Connell D and Gilmore B F 2012 *FEMS. Immunol. Med. Microbiol.* **65** 381
[19] Kang M H, Hong Y J, Attri P, Sim G B, Lee G J, Panngom K, Kwon G C, Choi E H, Uhm H S and Park G 2014 *Free Radical Biol. Med.* **72** 191
[20] Kaushik N, Kumar N, Kim C H, Kaushik N K and Choi E H 2014 *Plasma Process. Polym.* **11** 1175
[21] Davies K J A 1991 *Oxidative Damage and Repair: Chemical, Biological and Medical Aspects* (New York: Pergamon) pp 175–97, 261–81
[22] Fridman A and Friedman G 2013 *Plasma Medicine* (Oxford: Wiley) pp 115–20
[23] Birben E, Sahiner U M, Sackesen C, Erzurum S and Kalayci O 2012 *World Allergy Organ. J.* **5** 9
[24] Sies H 1985 *Oxidative Stress* (London: Academic) pp 15–27
[25] Thiyagarajan M, Waldbeser L and Whitmill A 2012 *Stud. Health Technol. Inform.* **173** 515
[26] Stoffels E, Sakiyama Y and Graves D B 2008 *IEEE Trans. Plasma Sci.* **36** 1441
[27] Hirst A M, Simms M S, Mann V M, Maitland N J, O'Connell D and Frame F M 2015 *Br. J. Cancer* **112** 1536
[28] Wei T, Chen C, Hou J, Xin W and Mori A 2000 *Biochim. Biophys. Acta* **1498** 72
[29] Murphy M P 1999 *Biochim. Biophys. Acta* **1411** 401
[30] Machala Z, Tarabova B, Hensel K, Spetlikova E, Sikurova L and Lukes P 2013 *Plasma Process. Polym.* **10** 649
[31] Martínez-Ruiz A, Cadenas S and Lamas S 2011 *Free Radical Biol. Med.* **51** 17
[32] Hogg N and Kalyanaraman B 1999 *Biochim. Biophys. Acta* **1411** 378
[33] Brune B 2003 *Cell Death Differ.* **10** 864
[34] Fry A 2010 *Electrochemistry in Medicine and Biomedical Applications* (Pennington, NJ: The Electrochemical Society) pp 1–15
[35] Lee G 2014 *Biomedical Engineering and Environmental Engineering* (Boston, MA: WIT) pp 330–40
[36] Kong M G, Kroesen G, Morfill G, Nosenko T, Shimizu T, van Dijk J and Zimmermann J L 2009 *New J. Phys.* **11** 115012
[37] Heinlin J, Isbary G, Stolz W, Morfill G, Landthaler M, Shimizu T, Steffes B, Nosenko T, Zimmermann J L and Karrer S 2011 *J. Eur. Acad. Dermatol. Venereol.* **25** 1
[38] Barekzi N and Laroussi M 2012 *J. Phys. D: Appl. Phys.* **45** 422002
[39] van Gils C A J, Hofmann S, Boekema B K H L, Brandenburg R and Bruggeman P J 2013 *J. Phys. D: Appl. Phys.* **46** 175203
[40] Fridman G, Shereshevsky A, Jost M M, Brooks A D, Fridman A, Vasilets A G V and Friedman G 2007 *Plasma Chem. Plasma Process* **27** 163
[41] Liu Ch, Dobrynin D and Fridman A 2014 *J. Phys. D: Appl. Phys.* **47** 252003
[42] Ayan H, Fridman G, Gutsol A F, Vasilets V N, Fridman A and Friedman G 2008 *IEEE Trans. Plasma Sci.* **36** 504
[43] Jiang P-C, Wang W-C, Zhang S, Jia L, Yang D-Z, Tang K and Liu Z-J 2014 *Spectrochim. Acta* A **122** 107
[44] Belinger A, Naudé N and Gherardi N 2014 *IEEE Trans. Plasma Sci.* **42** 2816
[45] Boeuf J P, Bernecker B, Callegari Th, Blanco S and Fournier R 2012 *Appl. Phys. Lett.* **100** 244108
[46] Yang Y, Cho Y I, Friedman G, Fridman A and Fridman G 2011 *IEEE Trans. Plasma Sci.* **39** 2060
[47] Callegari T, Bernecker B and Boeuf J P 2014 *Plasma Sources Sci. Technol.* **23** 054003
[48] Takashima (Udagawa) K, Zuzeek Y, Lempert W R and Adamovich I V 2011 *Plasma Sources Sci. Technol.* **20** 055009
[49] Norberg S A, Tian W, Johnsen E and Kushner M J 2014 *J. Phys. D: Appl. Phys.* **47** 475203
[50] NIST Thermophysical Properties of Fluid Systems, available at http://webbook.nist.gov/chemistry/fluid/
[51] Sander R 1999 Compilation of Henry's law constants for inorganic and organic species of potential importance in environmental chemistry, available at www.henrys-law.org/henry.pdf
[52] Mackay D and Shiu W Y 1981 *J. Phys. Chem. Ref. Data* **10** 1175
[53] Skyner R E, McDonagh J L, Groom C R, van Mourik T and Mitchell J B O 2015 *Phys. Chem. Chem. Phys.* **17** 6174
[54] Maddena K P and Mezyka S P 2011 *J. Phys. Chem. Ref. Data* **40** 023103
[55] NDRL/NIST Solution Kinetics Database, available at http://kinetics.nist.gov/solution/
[56] Pandis S N and Seinfeld J H 1989 *J. Geophys. Res.* **94** 1105
[57] Hudson R D 1971 *Rev. Geophys. Space Phys.* **9** 305
[58] Szabó C, Ischiropoulos H and Radi R 2007 *Nat. Rev. Drug Discovery* **6** 662
[59] Lukes P, Dolezalova E, Sisrova I and Clupek M 2014 *Plasma Sources Sci. Technol.* **23** 015019
[60] Atkinson R, Baulch D L, Cox R A, Crowley J N, Hampson R F, Hynes R G, Jenkin M E, Rossi M J and Troe J 2004 *Atmos. Chem. Phys.* **4** 1461
[61] Lindsay A, Anderson C, Slikboer E, Shannon S and Graves D B 2015 Momentum, heat and neutral mass transport in convective atmospheric pressure plasma-liquid systems and implications for aqueous targets *J. Phys.* D **48** 424007
[62] van Rens J F M, Schoof J T, Ummelen F C, van Vugt D C, Bruggeman P J and van Veldhuizen E M 2014 *Trans. Plasma Sci.* **42** 2622